Equilibrium energy spectrum of point vortex motion with remarks on ensemble choice and ergodicity

J. G. Esler*

Department of Mathematics, University College London, London WC1E 6BT, United Kingdom

(Received 19 August 2016; published 11 January 2017)

The dynamics and statistical mechanics of N chaotically evolving point vortices in the doubly periodic domain are revisited. The selection of the correct microcanonical ensemble for the system is first investigated. The numerical results of Weiss and McWilliams [Phys. Fluids A **3**, 835 (1991)], who argued that the point vortex system with $N = 6$ is nonergodic because of an apparent discrepancy between ensemble averages and dynamical time averages, are shown to be due to an incorrect ensemble definition. When the correct microcanonical ensemble is sampled, accounting for the vortex momentum constraint, time averages obtained from direct numerical simulation agree with ensemble averages within the sampling error of each calculation, i.e., there is no numerical evidence for nonergodicity. Further, in the $N \to \infty$ limit it is shown that the vortex momentum no longer constrains the long-time dynamics and therefore that the correct microcanonical ensemble for statistical mechanics is that associated with the entire constant energy hypersurface in phase space. Next, a recently developed technique is used to generate an explicit formula for the density of states function for the system, including for arbitrary distributions of vortex circulations. Exact formulas for the equilibrium energy spectrum, and for the probability density function of the energy in each Fourier mode, are then obtained. Results are compared with a series of direct numerical simulations with $N = 50$ and excellent agreement is found, confirming the relevance of the results for interpretation of quantum and classical two-dimensional turbulence.

DOI: 10.1103/PhysRevFluids.2.014703

I. INTRODUCTION

In a recent work Dritschel *et al.* [1] presented numerical calculations (for 10^2–10^3 vortices) showing that the equilibrium energy spectra of point vortex flows (on the sphere) vary smoothly with the total energy of the system. In simulations that were initialized out of equilibrium, moreover, the spectra relaxed to their equilibrium profiles at a rate proportional to the vortex collision time scale. These results strongly suggest that the point vortex equilibrium spectra are of considerable interest for understanding and interpreting freely evolving turbulence in those two-dimensional flows, whether classical, quantum, or plasma, in which the time scales associated with nonequilibrium processes (vortex mergers, annihilations, etc.) are longer than the relaxation time of the spectrum. Motivated by these considerations, the present work aims to show that the equilibrium spectra can be obtained analytically using a recently developed statistical mechanics framework [2]. Further, there is good agreement between the analytical equilibrium spectra and those observed in point vortex calculations.

Anticipating that our results will be relevant to both two-dimensional classical fluid turbulence (2DCT) and quantum turbulence (2DQT), the widely used doubly periodic domain is used for the present work, although the results should be straightforward to adapt to the sphere. While in certain limits both 2DCT and 2DQT can closely follow point vortex dynamics over finite-time periods, entirely different nonequilibrium processes occur in each system. A typical Navier-Stokes simulation of decaying 2DCT [3] is characterized by the formation of a population of coherent vortices. The vortex population evolves in time by merger and thinning events [4], believed to

*j.g.esler@ucl.ac.uk

be primarily due to three-body interactions [5,6], which result in the net transfer of energy to larger scales. The time-evolving distributions of vortex area and circulation of such emergent vortex populations have been demonstrated numerically to be predictable empirically [7,8]. By contrast, in Gross-Pitaevskii (defocusing nonlinear Schrödinger equations) simulations of 2DQT [9–11], vortices with quantized circulations are observed to form. Unlike in 2DCT, the vortex populations evolve by mutual annihilation of opposite signed vortices, also resulting in the net upscale transfer of energy.

The point vortex system is an idealized simple model for the study of the above systems and it remains an open question to determine the extent to which point vortices can be used to interpret 2DCT and 2DQT. Nevertheless, some encouraging results exist. For example, Billam *et al.* [9] in a study of 2DQT have found good agreement between Gross-Pitaevskii and point vortex energy spectra across a number of simulations at different energies. Preliminary calculations by Scott [12] suggest a similar level of agreement for the later stages of 2DCT simulations. Unlike in 2DCT or 2DQT, however, the vortex population in point vortex dynamics remains invariant in time. The point vortex equations are Hamiltonian, time reversible, and their solutions have a well-defined equilibrium energy spectrum [2] that depends only upon the conserved Hamiltonian or vortex interaction energy (VIE). A natural idea, following Onsager [13], is to use the methods of equilibrium statistical mechanics to understand the statistical organization of point vortices.

A quantitative approach to point vortex statistical mechanics, for the case of a general bounded domain, has been introduced recently by Esler and Ashbee (EA) [2]. Unlike the relatively-well-known sinh-Poisson or mean field theory (following Joyce and Montgomery [14]), which is known to provide reasonable predictions for the time-averaged mean flow end states of 2DCT flows [15], EA's theory is concerned with the statistics of the fluctuations of the turbulent flow. The theory of EA uses the central limit theorem, first to calculate the density of states function (a measure of the total number of microstates associated with a given VIE). From the density of states, statistics such as the equilibrium energy spectrum can be obtained, which can then be compared directly with those obtained from direct numerical simulations (DNSs) of the point vortex equations. The results hold for quite general distributions of vortex circulations. Comparison with DNS by EA showed that the calculated statistics are very accurate for $N = 100$ vortices and remain relevant for $N = 20$ or fewer. The results of EA generalize those of Pointin and Lundgren [16], obtained using the (cumbersome) cumulant expansion method for the special case of the doubly periodic domain with unit vortex circulations, to all bounded domains with arbitrary distributions of vortex circulations. Here we focus on extending the results of Ref. [16] and, more importantly, demonstrating the practical relevance of those results for the doubly periodic domain.

Applying the method of EA to the doubly periodic domain $\mathcal{D}$ is not trivial. For example, compared to bounded domains, $\mathcal{D}$ has both confounding and simplifying features that make a detailed treatment both necessary and of broader interest because of the implications for numerical studies of turbulence. Chief among these are the following.

(i) The results of EA are for bounded domain dynamics with no continuous symmetries. The only integral of the motion in these domains is the Hamiltonian (VIE). By contrast, due to the invariance of the dynamics under coordinate shifts in the direction of each axis, point vortex motion in $\mathcal{D}$ also "conserves" the vector-valued vortex momentum $\boldsymbol{P}$ (the reason for the quotation marks will be clarified below). The first aim of this work will be to explain the nature of $\boldsymbol{P}$ and to account for the curious lack of influence it exerts over the long-time statistics of either point vortex dynamics in the limit $N \to \infty$ or over those of Navier-Stokes dynamics with a continuous vorticity distribution.

(ii) It has been questioned in the literature whether or not the point vortex dynamics in $\mathcal{D}$ is ergodic, that is, do microcanonical ensemble averages agree with long-time averages of the dynamics? Weiss and McWilliams (WM) [17] addressed this question for $N = 6$ vortices in $\mathcal{D}$ and found disagreement between vortex separation statistics compiled from the microcanonical ensemble with those from long-time integrations of the equations of motion. Weiss and McWilliams interpreted this disagreement as evidence of nonergodicity, which in autonomous Hamiltonian dynamical systems typically indicates that phase space is partitioned into disjoint subspaces (cf. Birkhoff's theorem [18]),

with the dynamics confined to the subspace containing the initial conditions. Mysteriously, however, WM found no direct evidence of partitioning of phase space. The second aim of this work is therefore to revisit WM's calculations and show that, when the vortex momentum constraint is accounted for correctly, microcanonical and dynamical statistics agree to within calculated error bars. Based on these revised calculations, there is in fact no evidence of nonergodicity.

(iii) In contrast to the bounded domains discussed by EA, in the doubly periodic domain a key step in the derivation of the equilibrium statistics becomes analytically tractable, allowing explicit formulas to be found for, e.g., the density of states function. The third aim of this work is therefore to present these explicit formulas and describe a method for their efficient numerical evaluation. The validity of the energy spectrum results will be confirmed by comparison with DNS.

In addressing points (i)–(iii) above, a robust framework will be established for the use of equilibrium statistical mechanics for point vortices in $\mathcal{D}$ and a number of practical results will be established that should be of value to numerical modelers of 2DCT and 2DQT.

It is to be emphasized that it is not within the scope or spirit of this paper to address the mathematical question of formally proving ergodicity or nonergodicity in $\mathcal{D}$. In fact, it is known that at very high VIE the system is nonergodic, essentially because vortices can then be organized into a small number of tight clusters that can be shown to evolve arbitrarily close to the (deterministic) paths followed by their centroids. A formal proof on these lines using Kolmogorov-Arnold-Moser (KAM) theory exists by Khanin [19] for the case $N = 4$ and was extended to arbitrary N using a transformation to generalized Jacobi coordinates by Lim [20]. Notwithstanding these results, for researchers in turbulence the important question is whether nonergodic effects are significant enough at moderate (i.e. relevant) VIE to raise doubts over the application of methods from statistical mechanics. The present work aims to remove those doubts raised by WM and the existence of the vortex momentum constraint.

The plan of the work is as follows. In Sec. II the point vortex model is introduced, the vortex momentum $\boldsymbol{P}$ is defined, and its behavior under the dynamics is explained. The correct microcanonical ensemble for $\mathcal{D}$ is then defined and it is explained why $\boldsymbol{P}$ does not influence the dynamics in the limit $N \to \infty$. In Sec. III vortex separation statistics from the microcanonical ensemble with $N = 6$ are compiled and are then compared to time-averaged statistics from integrations of the point vortex equations. It is established that there is no numerical evidence for nonergodicity. In Sec. IV the equilibrium statistics for $N \to \infty$ are calculated, with explicit formulas obtained for the density of states function, the equilibrium energy spectrum, and the probability density functions (PDFs) of energy contained in each wave number. The results are tested against integrations of the point vortex equations with $N = 50$, with excellent agreement found. In Sec. V a summary is given and conclusions are drawn.

II. BACKGROUND: POINT VORTEX MOTION IN THE DOUBLY PERIODIC DOMAIN

A. Navier-Stokes equations in the doubly periodic domain

A useful starting point is to recall some general results for two-dimensional fluid dynamics in the doubly periodic domain $\mathcal{D}$ (here taken to be $(-\pi,\pi] \times (-\pi,\pi]$), before considering the point vortex limit below. In two dimensions the Navier-Stokes equations can be rewritten as an evolution equation for the vorticity $\omega(\boldsymbol{x},t)$,

$$(\partial_t + \boldsymbol{u} \cdot \boldsymbol{\nabla})\omega = \nu \nabla^2 \omega. \tag{1}$$

Here the fluid velocity $\boldsymbol{u} = -\boldsymbol{\nabla} \times \psi \boldsymbol{e}_z$, where $\boldsymbol{e}_z$ is the unit vector normal to the plane of motion, ψ is a stream function, and ν is the nondimensional viscosity (inverse of the Reynolds number). The stream function satisfies $\nabla^2 \psi = \omega$ or, alternatively,

$$\psi(\boldsymbol{x},t) = \int_{\mathcal{D}} G(\boldsymbol{x},\boldsymbol{x}')\omega(\boldsymbol{x}',t)d\boldsymbol{x}'. \tag{2}$$

In $\mathcal{D}$ the Green's function G in (2) has the formal expansion

$$G(\boldsymbol{x},\boldsymbol{x}') = -\sum_{\boldsymbol{k}} \frac{e^{i\boldsymbol{k}\cdot(\boldsymbol{x}-\boldsymbol{x}')}}{(2\pi k)^2}, \tag{3}$$

where $k = |\boldsymbol{k}|$ and the summation is over all integer wave-number pairs $\boldsymbol{k} = (k,l)^T$ except for $(0,0)^T$. Equation (3) shows that the velocity in $\mathcal{D}$ does not depend on the domain integral of ω, which is set to be zero without loss of generality.

The vorticity field also has a Fourier space representation

$$\omega(\boldsymbol{x}) = \omega_0 \sum_{\boldsymbol{k}} \Omega_{\boldsymbol{k}} e^{i\boldsymbol{k}\cdot\boldsymbol{x}}, \quad \Omega_{\boldsymbol{k}} = \frac{1}{(2\pi)^2\omega_0} \int_{\mathcal{D}} \omega(\boldsymbol{x}) e^{-\mathrm{i}\boldsymbol{k}\cdot\boldsymbol{x}} d\boldsymbol{x}. \tag{4}$$

Here (4), in which the summation again excludes (0,0), is standard except that the freedom in the definition of the Fourier transform is exploited to introduce a constant vorticity scale ω_0, which will prove useful as a bookkeeping device below. Notice that $\Omega_{\boldsymbol{0}} = 0$ because the domain integral of ω must remain zero in $\mathcal{D}$. The total fluid energy E_F in $\mathcal{D}$ can be written

$$E_F = -\frac{1}{2} \int_{\mathcal{D}^2} G(\boldsymbol{x},\boldsymbol{x}')\omega(\boldsymbol{x})\omega(\boldsymbol{x}') d\boldsymbol{x}\, d\boldsymbol{x}' = \frac{(2\pi)^4\omega_0^2}{2} \sum_{\boldsymbol{k}} \frac{|\Omega_{\boldsymbol{k}}|^2}{(2\pi k)^2}. \tag{5}$$

Further, using the fact that ω is a real function and that consequently $\Omega_{\boldsymbol{k}} = \Omega^*_{-\boldsymbol{k}}$, where the star denotes the complex conjugate, E_F can be written

$$E_F = (2\pi)^4\omega_0^2 {\sum_{\boldsymbol{k}}}' E_{\boldsymbol{k}}, \quad E_{\boldsymbol{k}} = \frac{|\Omega_{\boldsymbol{k}}|^2}{(2\pi k)^2}. \tag{6}$$

Here the primed summation denotes the sum over all integer pairs (k,l) with either $(k = 0, l > 0)$ or $k > 0$. It will be helpful to compare (6) with its point vortex equivalent below.

B. The point vortex limit and the vortex momentum constraint

Point vortex dynamics is a special case of (1) obtained by setting $\nu = 0$ and then considering the vorticity distribution

$$\omega(\boldsymbol{x}) = \sum_{i=1}^{N} \Gamma_i \delta(\boldsymbol{x} - \boldsymbol{x}_i), \tag{7}$$

where Γ_i is the circulation of the ith vortex, $\boldsymbol{x}_i = (x_i, y_i)^T$ denotes its position in $\mathcal{D}$, and $\delta(\cdot)$ is the Dirac delta. A well-known technical issue with point vortex dynamics is that the fluid energy E_F in (5) is then undefined. The system must be regularized by using instead a Hamiltonian energy H, which in $\mathcal{D}$ can be written in terms of the Green's function $G(\boldsymbol{x},\boldsymbol{x}')$ given by (3),

$$H(\boldsymbol{x}_1, \ldots, \boldsymbol{x}_N) = -\frac{1}{2} \sum_{i=1}^{N} \sum_{j=1, j\neq i}^{N} \Gamma_i \Gamma_j G(\boldsymbol{x}_i, \boldsymbol{x}_j). \tag{8}$$

Evolution equations [21] for the vortex positions can be derived from (1),

$$\Gamma_i \frac{dx_i}{dt} = -\frac{\partial H}{\partial y_i}, \quad \Gamma_i \frac{dy_i}{dt} = \frac{\partial H}{\partial x_i}, \quad i = 1, \ldots, N, \tag{9}$$

which are Hamilton's equations (up to a set of linear scaling factors). The Hamiltonian has no explicit time dependence and consequently H is an invariant of the dynamics. A natural rescaling for H,

which will prove convenient below, is

$$\bar{H} = \frac{H}{N\Gamma_0^2},$$

where

$$\Gamma_0 = \left(\frac{1}{N} \sum_{i=1}^{N} \Gamma_i^2 \right)^{1/2}$$

is the root-mean-square (rms) vortex circulation. The VIE ε is defined here to be the (conserved) value taken by $\bar{H}$ for a given dynamical run.

A key point to emphasize is that in $\mathcal{D}$ Eqs. (8) and (9) are invariant under vortex translations of the form $\boldsymbol{x}_i \to \boldsymbol{x}_i + 2\pi(m_i \boldsymbol{e}_x + n_i \boldsymbol{e}_y)$, where the (m_i, n_i) are arbitrary integers and $\boldsymbol{e}_x$ and $\boldsymbol{e}_y$ are, respectively, unit vectors in the x and y directions. In consequence, in the course of a dynamical integration vortex positions $\boldsymbol{x}_i$ can be constrained without loss of generality to lie within $\mathcal{D}$, i.e., it is possible to restrict $\boldsymbol{x}_i \in (-\pi, \pi] \times (-\pi, \pi]$ by applying the periodic boundary condition to add and subtract factors of 2π where necessary. In fact, for definiteness it is necessary to apply this restriction, in order that each spatial arrangement of vortices in $\mathcal{D}$ corresponds to a unique location in phase space.

The remaining vector-valued constant of the motion, identified by WM [17], is the vortex momentum $\boldsymbol{P} = P_x \boldsymbol{e}_x + P_y \boldsymbol{e}_y$, where

$$P_x = \sum_{i=1}^{N} \Gamma_i y_i, \quad P_y = -\sum_{i=1}^{N} \Gamma_i x_i.$$

Perhaps surprisingly, given that $\boldsymbol{P}$ can be defined analogously for the Navier-Stokes equations, aside from WM the vortex momentum has received little attention in the literature. The conservation of $\boldsymbol{P}$ is a consequence of the continuous symmetries of H under translation in the directions $\boldsymbol{e}_x$ and $\boldsymbol{e}_y$ (cf. Noether's theorem). To show this it is helpful to introduce the Poisson bracket

$$\{f, g\} = \sum_{i=1}^{N} \frac{1}{\Gamma_i} \left(\frac{\partial f}{\partial x_i} \frac{\partial g}{\partial y_i} - \frac{\partial f}{\partial y_i} \frac{\partial g}{\partial x_i} \right) \tag{10}$$

in terms of which Eqs. (9) are (using the overdot to denote time derivatives)

$$\dot{x}_i = \{x_i, H\}, \quad \dot{y}_i = \{y_i, H\}.$$

It is then easily verified (see the Appendix of WM [17]) that $\dot{P}_x = \{P_x, H\} = 0$ and $\dot{P}_y = \{P_y, H\} = 0$. The unusual property of P_x and P_y, recognized by WM, is that they are *not* conserved under the periodicity transformation $\boldsymbol{x}_i \to \boldsymbol{x}_i + 2\pi(m_i \boldsymbol{e}_x + n_i \boldsymbol{e}_y)$. When the restriction that $\boldsymbol{x}_i \in (-\pi, \pi] \times (-\pi, \pi]$ is imposed, as is necessary for definiteness, the consequence is that each time a vortex crosses a periodic boundary, either P_x or P_y will change in value.

In other words, $\boldsymbol{P}$ is not a conserved quantity in the commonly understood sense. For example, if $P_x(t = 0) = P_{0x}$, then at later times P_x will take values $P_{0x}^{\boldsymbol{m}}$ in the set

$$\left\{ P_{0x}^{\boldsymbol{m}} := P_{0x} + 2\pi m_i \Gamma_i | \boldsymbol{m} = (m_1, \ldots, m_N)^T \in \mathbb{Z}^N, -P_m < P_{0x}^{\boldsymbol{m}} < P_m \right\}. \tag{11}$$

Here $P_m = \pi \sum_i |\Gamma_i|$ is the maximum possible value for P_x (corresponding to all positive vortices at $x = \pi$ and all negative vortices at $x = -\pi$). Similar considerations naturally apply to P_y, i.e., if $P_y(t = 0) = P_{0y}$, P_y will subsequently take values $P_{0y}^{\boldsymbol{n}}$ in a set defined by analogy with (11).

That there is an equivalence between different points in the set of possible values taken by $\boldsymbol{P}$ is also clear from the following perspective. Consider a change in the coordinate system corresponding to a translation of the origin. As the origin is shifted, it follows from the fact that the domain integral of vorticity is zero that $\boldsymbol{P}$ is conserved until vortices cross the periodic boundaries, when its value

can jump to a different position in the set $(P_{0x}^{\boldsymbol{m}}, P_{0x}^{\boldsymbol{m}})$. From this perspective the specific value of $\boldsymbol{P}$ is relatively meaningless, because it is coordinate dependent, compared to its full set of accessible values, which is not.

Consider next the situation where one or more pairs of vortices have irrational circulation ratios (i.e., Γ_i/Γ_j is irrational for any i and j). In this case the set defined by (11) is dense on the open interval of the real line $-P_m < P_x < P_m$. Consequently, all possible values of P_x (and similarly P_y) will be accessible from any initial value $\boldsymbol{P} = \boldsymbol{P}_0$. As will be discussed below, the fact that all states are accessible has implications for the correct choice of the microcanonical ensemble (which in this case will be the ensemble of vortex arrangements with $\bar{H} = \varepsilon$). It is not correct, however, to conclude that in this case $\boldsymbol{P}$ has no role in the dynamics, because it may take a very large number of periodic boundary crossings, and therefore a very long time, to access a state with a given value of $\boldsymbol{P}$ from a given initial condition. It follows that the vortex momentum $\boldsymbol{P}$ can have a significant role in determining the time scale for ergodicity in the doubly periodic system, particularly when few vortices are present.

Now consider the case where the circulation ratios Γ_i/Γ_j are all rational. In this case the set (11) has a finite number of elements and during the course of the dynamics $\boldsymbol{P}$ will take values on a lattice. Consider, for simplicity, neutral gas examples with $\Gamma_i = \pm 1$ and $\sum_i \Gamma_i = 0$. Figure 1 compares the PDF of P_x when the vortices are arranged randomly (solid curves) with the accessible values, i.e., those in the set (11), for two different initial conditions: $P_{0x} = 0$ (red lines) and $P_{0x} = \pi$ (blue lines). The top panel shows the case with $N = 6$ and the bottom panel $N = 50$ (details of the calculation are given in Appendix A). Naturally, the same picture applies to P_y, therefore a given initial condition $\boldsymbol{P}(0) = \boldsymbol{P}_0$ restricts $\boldsymbol{P}(t)$ to subsequently take values on a two-dimensional lattice. However, for the $N = 50$ case, the lattice for $\boldsymbol{P}(t)$ appears dense in Fig. 1(b) and might be expected to serve as a reasonably accurate discretization of the continuous distribution. Hence, for $N = 50$ one might expect the influence of the initial value of $\boldsymbol{P}$ to be very weak and this is indeed what is found in our statistical sampling study below. It follows that in the limit $N \to \infty$ the influence of $\boldsymbol{P}_0$ on the statistics will become negligible.

C. Statistical mechanics preliminaries

The point vortex system is an isolated Hamiltonian system and its statistics are therefore those of the microcanonical ensemble. The microcanonical ensemble is defined to be the set of all microstates (vortex arrangements) that are consistent with the invariants of the motion. In the doubly periodic domain the relevant invariants are the VIE ε and the vortex momentum $\boldsymbol{P}$.

In the case with irrational circulation ratios or with large N, the vortex momentum $\boldsymbol{P}$ does not constrain the motion and the microcanonical ensemble consists of all microstates with VIE equal to ε. The microcanonical ensemble average of any quantity $Q(\boldsymbol{x}_1, \ldots, \boldsymbol{x}_N)$ is then defined to be

$$\langle Q \rangle = \frac{1}{(2\pi)^{2N}} \int_{\mathcal{D}^N} Q(\boldsymbol{x}_1, \ldots, \boldsymbol{x}_N)\, p_\varepsilon(\boldsymbol{x}_1, \ldots, \boldsymbol{x}_N)\, d\boldsymbol{x}_1 \cdots d\boldsymbol{x}_N, \tag{12}$$

where the microcanonical probability p_ε can be written

$$p_\varepsilon(\boldsymbol{x}_1, \ldots, \boldsymbol{x}_N) = \frac{\delta(\bar{H}(\boldsymbol{x}_1, \ldots, \boldsymbol{x}_N) - \varepsilon)}{(2\pi)^{2N} W(\varepsilon)}. \tag{13}$$

The normalizing function appearing in (13),

$$W(\varepsilon) = \frac{1}{(2\pi)^{2N}} \int_{\mathcal{D}^N} \delta(\bar{H}(\boldsymbol{x}_1, \ldots, \boldsymbol{x}_N) - \varepsilon) d\boldsymbol{x}_1 \cdots d\boldsymbol{x}_N, \tag{14}$$

is known as the density of states function and is key to the development of our results in Sec. IV below. The function $W(\varepsilon)$ can itself be interpreted as a PDF, namely, the PDF of $\bar{H}$ when the vortices are arranged randomly in $\mathcal{D}$ (i.e., under the uniform ensemble). Notably, following EA,

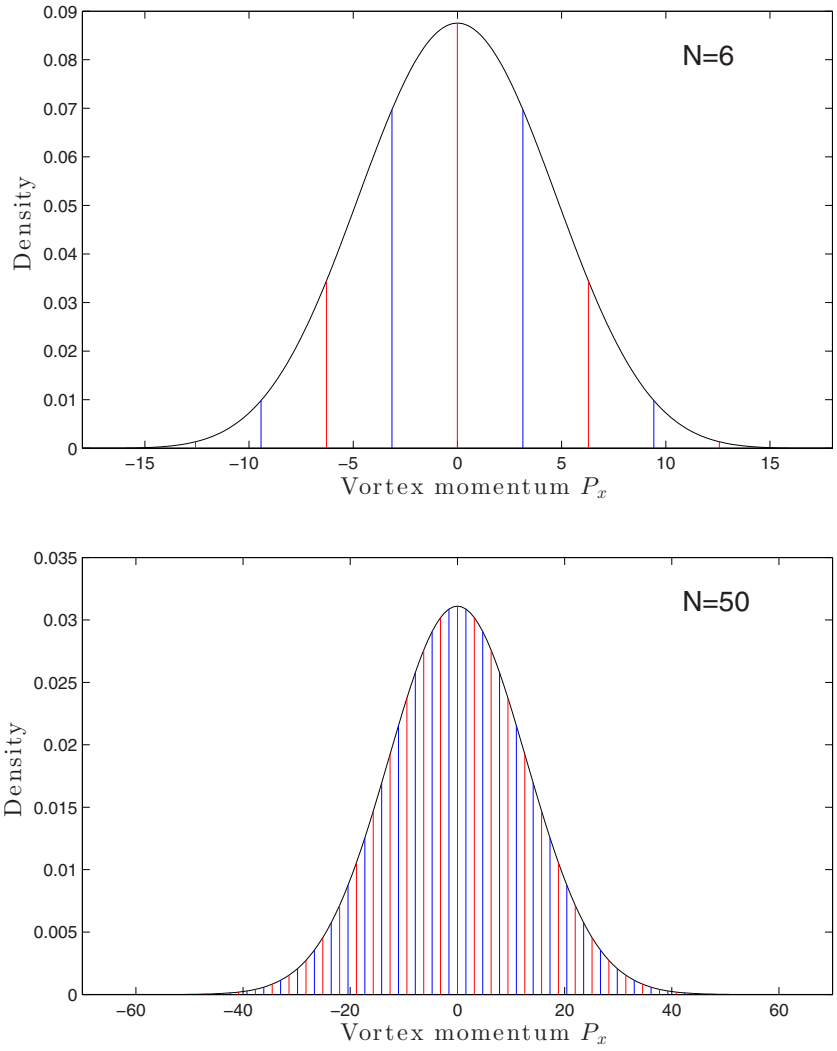

FIG. 1. Solid curves show the density of P_x under the uniform ensemble for $N = 6$ vortices (top) and $N = 50$ vortices (bottom). Equal numbers have circulation $\Gamma_i = \pm 1$ in both cases. The red lines are the values of P_x accessible from initial condition $P_{0x} = 0$ and the blue lines the values of P_x accessible from initial condition $P_{0x} = \pi$.

under a few mild restrictions on the limiting behavior of $\mathbf{\Gamma} = (\Gamma_1, \ldots, \Gamma_N)^T$ (the distribution of vortex circulations), $W(\varepsilon)$ can be shown to be independent of $\mathbf{\Gamma}$ in the limit $N \to \infty$.

In the case where the circulation ratios are all rational (e.g., in the $N = 6$ vortex problem of WM to be discussed below), then the vortex momentum $\boldsymbol{P}$ cannot be neglected in the microcanonical ensemble. In this case p_ε in (12) must be replaced by

$$\tilde{p}_\varepsilon(\boldsymbol{x}_1, \ldots, \boldsymbol{x}_N) = \sum_{(\boldsymbol{m},\boldsymbol{n})} \frac{\delta\left(\boldsymbol{P}(\boldsymbol{x}_1, \ldots, \boldsymbol{x}_N) - \boldsymbol{P}_0^{(\boldsymbol{m},\boldsymbol{n})}\right) \delta(\bar{H}(\boldsymbol{x}_1, \ldots, \boldsymbol{x}_N) - \varepsilon)}{(2\pi)^{2N} W(\varepsilon, \boldsymbol{P}_0)}. \tag{15}$$

The summation in (15) is over all lattice points $\boldsymbol{P}_0^{(\boldsymbol{m},\boldsymbol{n})} = (P_{0x}^{\boldsymbol{m}}, P_{0y}^{\boldsymbol{n}})^T$ in the set (11), which are generated by the vortex momentum initial condition $\boldsymbol{P}_0 = (P_{0x}, P_{0y})^T$. Finally, $W(\varepsilon, \boldsymbol{P}_0)$ is a

generalized density of states function defined by analogy with (14). Below, ensemble averages based on (15) will be denoted by $\langle\cdot\rangle_{\boldsymbol{P}}$. Based on the discussion of Sec. II B above, it follows that for a quantity Q, (i) $\langle Q\rangle_{\boldsymbol{P}} = \langle Q\rangle$ when the ratio of vortex circulations Γ_i/Γ_j is irrational for any i and j and (ii) $\langle Q\rangle_{\boldsymbol{P}} \to \langle Q\rangle$ in the limit $N \to \infty$. Numerical verification of these results will be presented below.

Weiss and McWilliams (implicitly) use a different definition of the microcanonical ensemble, because they sample states with vortex momentum equal to its initial value only, i.e., in place of (15) they use

$$\hat{p}_\varepsilon(\boldsymbol{x}_1,\ldots,\boldsymbol{x}_N) = \frac{\delta(\boldsymbol{P}(\boldsymbol{x}_1,\ldots,\boldsymbol{x}_N)-\boldsymbol{P}_0)\delta(\bar{H}(\boldsymbol{x}_1,\ldots,\boldsymbol{x}_N)-\varepsilon)}{(2\pi)^{2N}\widehat{W}(\varepsilon,\boldsymbol{P}_0)}. \tag{16}$$

This definition is incorrect because, in the dynamics, all lattice points defined by (11) are accessible from the initial state. The ensemble averages from WM's ensemble will be denoted by $\langle\cdot\rangle_{\mathrm{WM}}$ below. The incorrect definition (16) will be shown below to account for WM's conclusion of nonergodicity.

Before progressing to our main results below, it is helpful to develop the relationship between $\bar{H}$ and the discrete fluid dynamical energy spectrum (6), following Sec. 3 of [22]. First note that an alternative expression for (8) is

$$H = -\frac{1}{2}\int_{\mathcal{D}^2} G(\boldsymbol{x},\boldsymbol{x}')[\omega(\boldsymbol{x})\omega(\boldsymbol{x}') - R(\boldsymbol{x},\boldsymbol{x}')]d\boldsymbol{x}\,d\boldsymbol{x}', \tag{17}$$

where ω is given by the distribution (7) and R by the distribution

$$R(\boldsymbol{x},\boldsymbol{x}') = \sum_{i=1}^{N}\Gamma_i^2\delta(\boldsymbol{x}-\boldsymbol{x}_i)\delta(\boldsymbol{x}'-\boldsymbol{x}_i). \tag{18}$$

It is straightforward to verify that (17) is equivalent to (8) by inserting the distributions for ω and R and evaluating the integral. The distribution R also has a Fourier expansion

$$R(\boldsymbol{x},\boldsymbol{x}') = \sum_{\boldsymbol{k}}\sum_{\boldsymbol{k}'} R_{\boldsymbol{k}\boldsymbol{k}'}e^{i(\boldsymbol{k}\cdot\boldsymbol{x}+\boldsymbol{k}'\cdot\boldsymbol{x}')},$$

$$R_{\boldsymbol{k}\boldsymbol{k}'} = \frac{1}{(2\pi)^4}\int_{\mathcal{D}^2} R(\boldsymbol{x},\boldsymbol{x}')e^{-i(\boldsymbol{k}\cdot\boldsymbol{x}+\boldsymbol{k}'\cdot\boldsymbol{x}')}d\boldsymbol{x}\,d\boldsymbol{x}' = \frac{1}{(2\pi)^4}\sum_{i=1}^{N}\Gamma_i^2 e^{-i(\boldsymbol{k}+\boldsymbol{k}')\cdot\boldsymbol{x}_i}. \tag{19}$$

Equation (17) is in a form that allows the Fourier expansions (4), (19), and (3) to be inserted and the resulting integrals evaluated to give

$$H = \frac{(2\pi)^4}{2}\sum_{\boldsymbol{k}}\frac{\omega_0^2|\Omega_{\boldsymbol{k}}|^2 - R_{\boldsymbol{k},-\boldsymbol{k}}}{(2\pi k)^2}. \tag{20}$$

A simplification follows because, from (19), $R_{\boldsymbol{k},-\boldsymbol{k}} = N\Gamma_0^2/(2\pi)^4$ is a constant. If the hitherto unspecified vorticity scale is now chosen to be $\omega_0 = N^{1/2}\Gamma_0/(2\pi)^2$ it follows that $\bar{H} = H/N\Gamma_0^2$ can be written

$$\bar{H} = \varepsilon = {\sum_{\boldsymbol{k}}}' \frac{|\Omega_{\boldsymbol{k}}|^2 - 1}{(2\pi k)^2} = {\sum_{\boldsymbol{k}}}' E_{\boldsymbol{k}} - \langle E_{\boldsymbol{k}}\rangle_0. \tag{21}$$

Here $E_{\boldsymbol{k}}$ is the (scaled) energy in wave number $\boldsymbol{k}$, exactly as appears in the continuous case (6). The additional term $\langle E_{\boldsymbol{k}}\rangle_0 = (2\pi k)^{-2}$ is precisely the energy expected in wave number $\boldsymbol{k}$ had the vortices been arranged randomly in $\mathcal{D}$ under uniform measure. The result (21) defines a relationship between the point vortex energy spectrum, the vortex interaction energy ε, and the fluid dynamical energy spectrum, which will be discussed further below.

III. ERGODICITY AND THE ROLE OF P IN THE DOUBLY PERIODIC DOMAIN

In this section the study of WM, which concluded that the point vortex system is nonergodic, is revisited. In particular, a direct comparison is made between statistics obtained from DNS of the point vortex equations (9) and statistics obtained by sampling the microcanonical ensemble (12). No evidence for nonergodicity is found, as will be described next.

A. Numerical integration of the point vortex equations

To repeat the study of WM it is necessary to integrate the point vortex equations (9) numerically. An eighth-order adaptive Runge-Kutta time-stepping algorithm [23] is used. A high-order adaptive method is advantageous because of intermittent periods during which pairs of vortices pass close together [24]. Such periods require much shorter time steps than is typical. To efficiently evaluate the velocities from the vortex positions $\{\boldsymbol{x}_1,\ldots,\boldsymbol{x}_N\}$ in (9) it is first necessary to express the Green's function (3) in a form allowing inexpensive evaluation. Several rapidly converging expressions are available (see [25,26] as well as [17]). The method of WM is used here. A brief discussion of some details is given in Appendix B.

We have performed long integrations (duration $10^5\Gamma_0^{-1}$–$10^6\Gamma_0^{-1}$) with both $N=6$ vortices of unit circulation (3 positive, 3 negative) and with $N=50$ (25 positive, 25 negative). Each run is initialized with randomly generated initial conditions, which have different values of the Hamiltonian $\bar{H}=\varepsilon$ (detailed below) and different values of the vortex momentum [typically $\boldsymbol{P}_0=(0,0)^T,(\pi,0)^T,(\pi,\pi)^T$]. The runs are sufficiently long that the influence of ε and $\boldsymbol{P}_0$ on the long-time statistics can be determined.

Key tests of numerical accuracy are if (i) $\bar{H}$ is conserved during the integration and (ii) the vortex momentum $\boldsymbol{P}(t)$ takes values on the lattice defined by (11). Our code is structured so that the accuracy of conservation is governed indirectly by a tolerance parameter $\delta_{\Delta t}$ for the rms error in vortex positions over integration intervals Δt. For most of the time during our integrations $\Delta t=\Gamma_0^{-1}$ and $\delta_{\Delta t}=10^{-8}$. However, a further level of adaptivity is built into the code. If $\bar{H}$ is not conserved to within a tolerance δ_H (typically $\delta_H=10^{-8}$ is used) over a given time interval $[t,t+\Delta t]$, as occasionally occurs because of unusual interactions of nearby vortices, the integration interval is repeated with $\delta_{\Delta t}$ reduced by an order of magnitude. This extra level of adaptivity ensures close control over the cumulative error in $\bar{H}$ over the length of the integration. Note that errors in $\bar{H}$ are found to be biased so that there is drift towards $\bar{H}=0$ (maximum entropy).

A typical cumulative numerical error in conservation of $\bar{H}$ for a $t=10^6\Gamma_0^{-1}$ run with $N=6$ is less than $1\times10^{-4}\sigma_\varepsilon$, where $\sigma_\varepsilon^2=\langle\bar{H}^2\rangle_0$ is the variance of $\bar{H}$ under the uniform ensemble (random arrangement of vortices in $\mathcal{D}$). For $N=6$ the standard deviation is $\sigma_\varepsilon=0.0401$ (three significant figures). The error is therefore considerably less than the width of an energy shell used for sampling the microcanonical ensemble below. A typical error in $\bar{H}$ for a run of length $t=5\times10^5\Gamma_0^{-1}$ with $N=50$ is somewhat larger, at $2\times10^{-3}\sigma_\varepsilon$, where in this case $\sigma_\varepsilon=0.0440$ (a value that is in agreement to three significant figures with the $N\to\infty$ prediction calculated below).

Figure 2 shows snapshots of vortex positions at late times during DNS with $N=50$. The snapshots illustrate the extent to which the distribution of vortices is influenced by the VIE ε. The left panel shows a run with $\varepsilon=-2\sigma_\varepsilon$, which is in the positive temperature dipole-forming regime; the center panel shows $\varepsilon=0$, which is near maximum entropy for the system; and the right panel shows $\varepsilon=5\sigma_\varepsilon$, in the negative temperature regime characterized by the formation of like-signed clusters.

Figure 3 shows the evolution of x-vortex momentum $P_x(t)$ during two simulations with $N=6$ (top panel) and two with $N=50$ (bottom panel). In each case the simulations differ in the initial value of $P_x(0)=P_{0x}$, with the solid black curves corresponding to $P_{0x}=0$ and the dashed gray curves to $P_{0x}=\pi$. Evidently, during the evolution $P_x(t)$ jumps between the lattice points of (11) as anticipated in the discussion of Sec. II B. Compared with the $N=6$ runs, the $N=50$ runs are distinguished by (as should be expected) a much greater frequency of periodic boundary crossings and consequent jumps between lattice points. The much greater density of lattice points in the $N=50$ case (cf. Fig. 1) is also apparent.

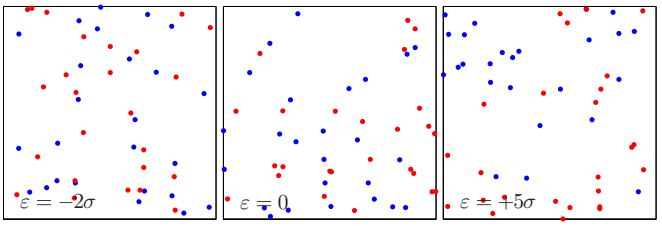

FIG. 2. Snapshot of vortex positions at late times from DNS with $N = 50$ ($\Gamma_i = \pm 1$, 25 positive are blue, 25 negative are red). DNS with three different VIE are shown: $\varepsilon = -2\sigma_\varepsilon$ (left), $\varepsilon = 0$ (middle), and $\varepsilon = +5\sigma_\varepsilon$ (right).

B. Numerical sampling of the microcanonical ensemble for $N = 6$

To investigate ergodicity the microcanonical ensemble defined in Sec. II C must be sampled numerically. In the interest of avoiding any possible sources of ambiguity or sampling bias a direct brute force sampling method is used for the $N = 6$ vortex case. The PDF (15) is first smoothed by replacing the energy δ function by an energy shell of width $\delta_\varepsilon = \sigma_\varepsilon/30$ and the vortex momentum δ function by a small box of width $\delta_p = 0.01$. Sampling proceeds by the repeated process of sampling from a set of six identical independent random variables $\{X_1, X_2, X_3, X_4, X_5, X_6\}$, which are uniformly distributed in $(-\pi, \pi]$. A sampled set is deemed accepted and recorded, as a possible

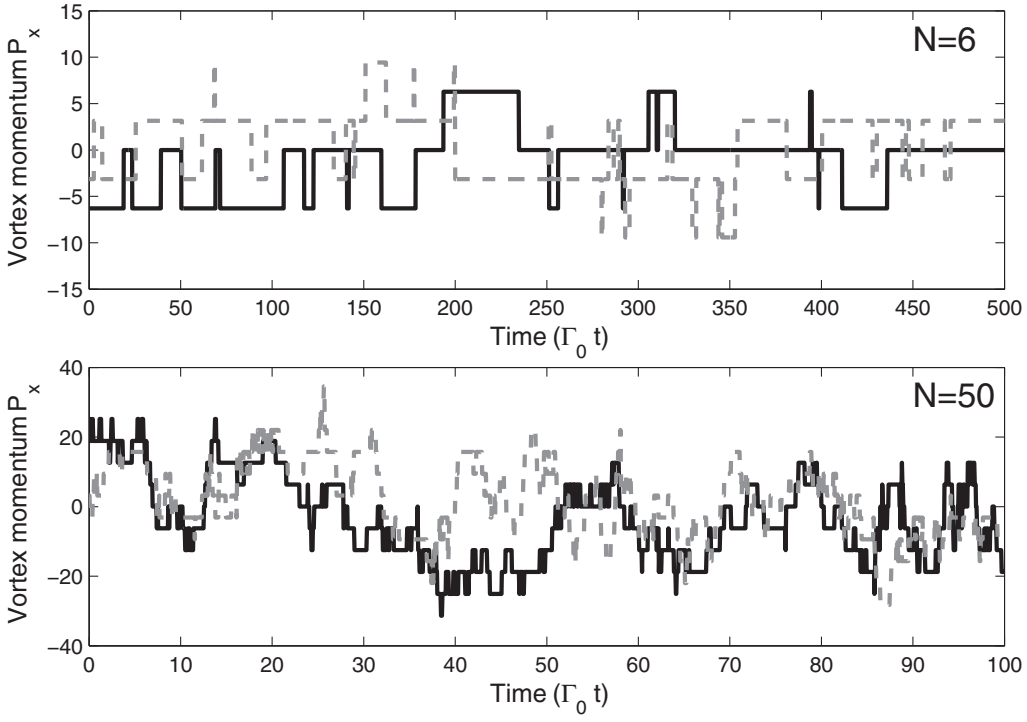

FIG. 3. Time evolution of x-vortex momentum $P_x(t)$ in numerical integrations with $N = 6$ (top) and $N = 50$ (bottom). Solid black curves show runs with initial vortex momentum $P_x(0) = P_{0x} = 0$ and dashed gray curves show runs with $P_x(0) = P_{0x} = \pi$ (note that $t = 0$ in the figure does not correspond to the beginning of the runs).

set of x coordinates for the vortices, if the condition

$$\left(P_{0x}^{\boldsymbol{m}} - \sum_{i=1}^{6} \Gamma_i X_i\right)^2 \leqslant \delta_p^2 \tag{22}$$

is met for any $P_{0x}^{\boldsymbol{m}}$ in the set (11). The value $\delta_p = 0.01$ is found to be an acceptable small distance to a nearby lattice point, because calculations have been repeated with δ_p both doubled and halved without a significant change in the results. The process is repeated, using $P_{0y}^{\boldsymbol{n}}$ in place of $P_{0x}^{\boldsymbol{m}}$ to generate sets of possible y coordinates. Following this process, a large number (of order 10^8) of sets of vortex configurations consistent with the initial vortex momentum $\boldsymbol{P}_0 = P_{0x}\boldsymbol{e}_x + P_{0y}\boldsymbol{e}_y$ are found.

The next step is to repeatedly select sets of x and y coordinates at random from the compiled list and calculate the Hamiltonian energy $\bar{H}$ for each resulting vortex configuration. When the energy falls within the energy shell of interest (i.e., $\bar{H} \in [\varepsilon - \delta_\varepsilon/2, \varepsilon + \delta_\varepsilon/2]$) the configuration is accepted as an ensemble member and the statistics of interest are recorded. Typically, the statistics reported below are compiled from 10^6–10^7 ensemble members.

The sampling process described above differs from that of WM in that all lattice points of $\boldsymbol{P}$ consistent with the initial conditions $\boldsymbol{P}_0$ are sampled. Weiss and McWilliams sampled only vortex configurations associated with the original lattice point $\boldsymbol{P}_0$. The subset of our samples associated with this original lattice point were also recorded and used to generate statistics for WM's ensemble described below.

C. Comparison of DNS time averages and ensemble averages

The main test of ergodicity employed by WM was to investigate the statistics of the (vorticity-weighted) vortex separations

$$p(r) = \langle \delta(r - |\boldsymbol{x}_i - \boldsymbol{x}_j|)\rangle, \quad q(r) = \langle \Gamma_i \Gamma_j \delta(r - |\boldsymbol{x}_i - \boldsymbol{x}_j|)\rangle, \tag{23}$$

where a summation is implied over all distinct vortex pairs (i, j) and the angular brackets denote either the ensemble average (12) or time averages from the DNS. The physical meaning of these statistics is discussed by WM.

Here the statistics of $p(r)$ and $q(r)$ are generated using a histogram method, compiled from (i) periodic sampling of DNS output or (ii) vortex configurations drawn from the microcanonical ensemble (see above). As in the work of WM [17], error bars due to finite sample sizes can be obtained using subsampling.

A key piece of evidence for nonergodicity in the work of WM [17] is their Fig. 3(b), where $q(r)$ is plotted for a run[1] with $\varepsilon = -0.442\sigma_\varepsilon$ and $\boldsymbol{P}_0 = \boldsymbol{0}$. Compared with $q(r)$ calculated from the microcanonical ensemble, a discrepancy is seen that is many times greater than that expected through sampling error. To show that WM's result is due to using the incorrect ensemble definition (16), instead of (15), we have reproduced WM's calculation as accurately as possible. Figure 4 shows $q(r)$ from our calculations, showing (i) the time average from DNS, (ii) the correct microcanonical average $\langle\cdot\rangle_{\boldsymbol{P}}$, and (iii) the Weiss-McWilliams ensemble average $\langle\cdot\rangle_{\mathrm{WM}}$. First, it is clear that, within the error bars due to sampling error, there is no discernible difference between the DNS time average of $q(r)$ and the microcanonical average $\langle\cdot\rangle_{\boldsymbol{P}}$. Second, WM's results are accurately reproduced, as the discrepancy between the time average and the Weiss-McWilliams ensemble average $\langle\cdot\rangle_{\mathrm{WM}}$ is more or less identical to that shown in Fig. 3(b) of [17].

[1]The discrepancy in the value of ε given here compared to that given by WM occurs because the uniform ensemble is used to define the mean and standard deviation of $\bar{H}$ in our work, whereas the Weiss-McWilliams ensemble defined by (16) is used in [17].

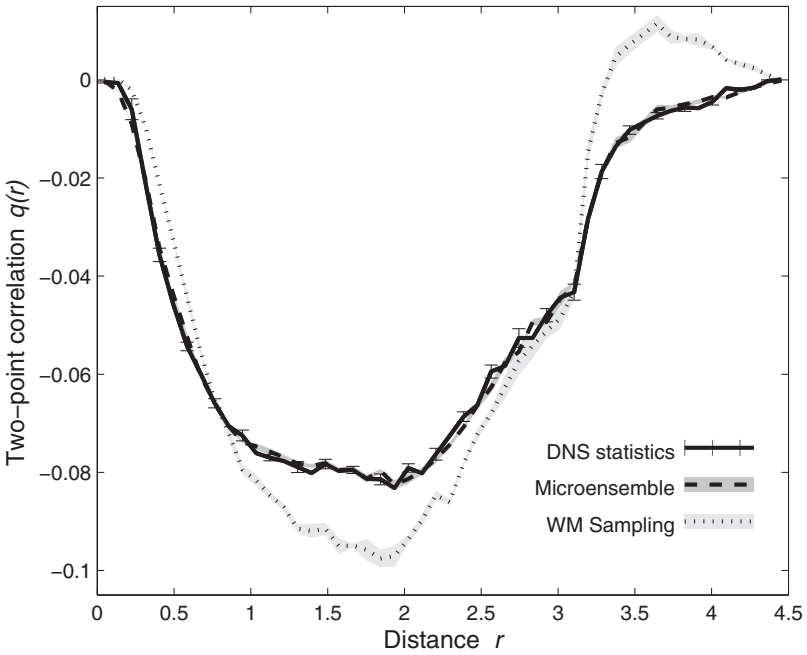

FIG. 4. Vorticity-weighted vortex separation $q(r)$ in (i) the DNS time average (solid curve with error bars), (ii) the microcanonical ensemble average $\langle\cdot\rangle_{\boldsymbol{P}}$ defined by (15) (dashed curve with gray shading), and (iii) the Weiss-McWilliams ensemble average $\langle\cdot\rangle_{\mathrm{WM}}$ defined by (16) (dotted curve with light gray shading).

Similarly convincing agreement between time averages and $\langle\cdot\rangle_{\boldsymbol{P}}$ has also been obtained in further calculations over a range of values of ε and $\boldsymbol{P}_0$. Our conclusion is therefore that, at the level of numerical evidence that is obtainable in practice for the $N = 6$ system, there is no evidence for nonergodicity of the point vortex system.

D. Role of the vortex momentum $\boldsymbol{P}$

Does the vortex momentum $\boldsymbol{P}$ ever have a significant influence on the vortex statistics? Situations where $\boldsymbol{P}$ has no role have been highlighted above (e.g., irrational circulation ratios $N \to \infty$). It is therefore of interest to quantify the extent to which the initial value of $\boldsymbol{P}$ can influence the time-averaged statistics of our $N = 6$ calculations. The statistics of long DNS calculations of (9) have been compiled from three runs with (i) $\boldsymbol{P}_0 = (0,0)$, (ii) $\boldsymbol{P}_0 = (\pi,0)$, and (iii) $\boldsymbol{P}_0 = (\pi,\pi)$, respectively. Notice that when $\Gamma_i = \pm 1$, changes in P_{0x} of $\pm 2\pi$ are equivalent to jumping to adjacent lattice points (cf. Fig. 3). The initial values (i)–(iii) above therefore represent the maximum possible displacements of the lattices of accessible values of $\boldsymbol{P}$ generated by $\boldsymbol{P}_0$. The differences between the statistics of runs (i)–(iii) therefore represent the maximum possible influence of $\boldsymbol{P}$.

Figure 5 shows how the vorticity weighted vortex separation $q(r)$ depends on $\boldsymbol{P}$. In the left panel, showing the $N = 6$ runs, it is clear that the influence of $\boldsymbol{P}$ is modest but noticeable. As a point of comparison, a change in the initial value of the Hamiltonian $\bar{H}$ of $\pm\sigma_\varepsilon$ is sufficient to change the profile of $q(r)$ by an amount significantly greater than the differences seen in Fig. 5, as can be seen in Figs. 3–7 of [17]. Therefore, even with as few as six vortices, $\boldsymbol{P}_0$ has a minor role compared to ε in influencing the statistics.

The right panel presents the results from the $N = 50$ runs and shows that the influence of $\boldsymbol{P}_0$ is near negligible, as anticipated. The lattice points $\boldsymbol{P}_0^{(m,n)}$ generated by $\boldsymbol{P}_0$ are sufficiently dense to act as a good approximation to the distribution of $\boldsymbol{P}$ under the uniform distribution, regardless of the exact value of $\boldsymbol{P}_0$. This result justifies neglecting consideration of $\boldsymbol{P}$ in the statistical mechanics

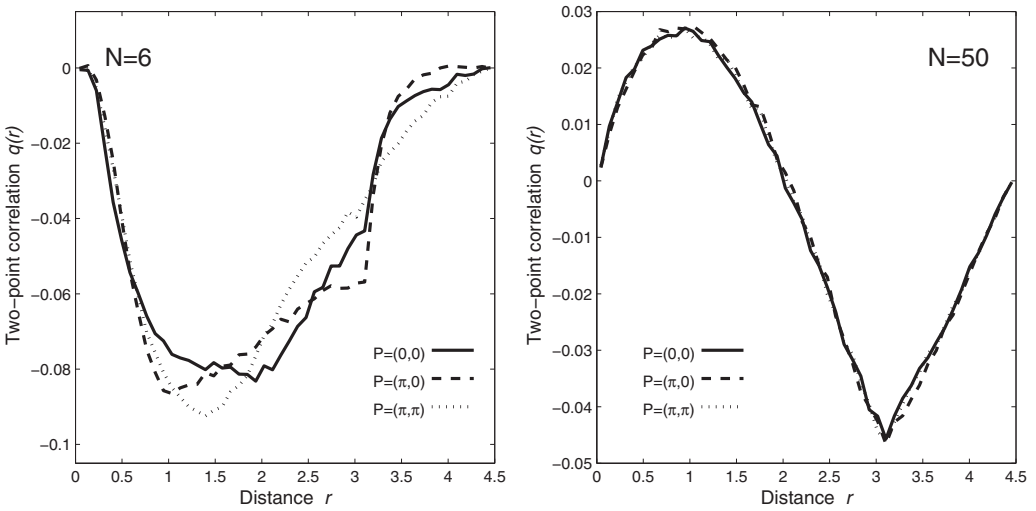

FIG. 5. Shown on the left is the average vorticity-weighted vortex separation $q(r)$ for $N = 6$ runs with $\varepsilon = -0.442\sigma_\varepsilon$ and (i) $\boldsymbol{P}_0 = (0,0)$ (solid curve), (ii) $\boldsymbol{P}_0 = (\pi,0)$ (dashed curve), and (iii) $\boldsymbol{P}_0 = (\pi,\pi)$ (dotted curve). The right side is the same as the left but for $N = 50$ vortices, at $\varepsilon = 0$.

approach for large N below [i.e., using Eq. (13) in place of Eq. (15)] and indicates that in practice it is safe to do so for a relatively modest number of vortices.

IV. EQUILIBRIUM ENERGY SPECTRUM

Next the statistical theory for the equilibrium energy spectrum, and some related statistics, will be developed. The theory is formally valid in the limit $N \to \infty$ and consequently, based on the theory of Sec. II B, the influence of the vortex momentum $\boldsymbol{P}$ can be neglected without loss of validity. The approach taken is similar to that of EA with one major difference in the outcome, which is that an analytical formula is obtained for the density of states function and by extension for the equilibrium energy spectrum itself.

A. Evaluation of the density of states function

The first step in our statistical theory is to obtain a formula for the density of states $W(\varepsilon)$ defined by (14) above. To proceed, it is helpful to interpret $W(\varepsilon)$ as the PDF of the normalized Hamiltonian $\bar{H}$, under the uniform ensemble. The uniform ensemble is defined to be the set of all possible vortex configurations under uniform measure in $\mathcal{D}$ and its statistics can be obtained by sampling each vortex location $\boldsymbol{X}_i$ as a random variable uniformly distributed over $\mathcal{D}$.

When the number of vortices $N \to \infty$ the method of EA, based on the central limit theorem (CLT), can be used to evaluate $W(\varepsilon)$. As discussed by EA [2], some assumptions are necessary. The simplest treatment assumes a fixed ratio neutral vortex gas, which is defined as follows. When taking the limit $N \to \infty$, a fixed ratio α_j of the vortices is taken to have a constant circulation $\bar{\Gamma}_j$, where $j = 1, \ldots, J$ and $J < \infty$ is the number of different vortex populations. Evidently, $\sum_{j=1}^{J} \alpha_j = 1$. Note that, because time can be rescaled in the equations of motion, the circulations $\bar{\Gamma}_j$ can be constant or, provided their ratios remain fixed, can multiply an arbitrary function of N without affecting the argument below. The condition of neutrality (no net circulation), which is necessary in $\mathcal{D}$, is

$$\sum_{j=1}^{J} \alpha_j \bar{\Gamma}_j = 0. \tag{24}$$

The rms circulation introduced above is

$$\Gamma_0 = \left(\sum_{j=1}^{J} \alpha_j \bar{\Gamma}_j^2 \right)^{1/2}. \tag{25}$$

Notice that, for the $N = 6$ and $N = 50$ integrations under discussion, the vortex distribution corresponds to the special case of a uniform neutral vortex gas [2,27], for which $J = 2$ and $\alpha_{1,2} = 1/2$.

The key to progress is to first determine the distribution of the Fourier components $\Omega_{\boldsymbol{k}}$ under the uniform ensemble. To do so, $\Omega_{\boldsymbol{k}}$ is first decomposed into contributions from each of the J vortex populations as

$$\Omega_{\boldsymbol{k}} = \sum_{j=1}^{J} \frac{\alpha_j^{1/2}}{2^{1/2}} \frac{\bar{\Gamma}_j}{\Gamma_0} \Omega_{\boldsymbol{k}}^j, \quad \Omega_{\boldsymbol{k}}^j = \frac{1}{(\alpha_j N)^{1/2}} \sum_{i=i_j+1}^{i_j+\alpha_j N} 2^{1/2} e^{-i\boldsymbol{k}\cdot\boldsymbol{X}_i}, \tag{26}$$

where $i_j + 1$ here denotes the first index of the jth population. Notice that the real and imaginary parts of $\Omega_{\boldsymbol{k}}^j$ correspond to sums of random variables that have zero mean and unit variance. Next, applying the CLT to the formula for $\Omega_{\boldsymbol{k}}^j$ results in

$$\Omega_{\boldsymbol{k}}^j = A_{\boldsymbol{k}}^j + i B_{\boldsymbol{k}}^j, \quad A_{\boldsymbol{k}}^j, B_{\boldsymbol{k}}^j \sim \mathcal{N}(0,1). \tag{27}$$

Here $\mathcal{N}(\mu,\sigma^2)$ denotes the Gaussian distribution with mean μ and variance σ^2. That the $\{A_{\boldsymbol{k}}^j\}$ and $\{B_{\boldsymbol{k}}^j\}$ are independent follows from the orthogonality of the Fourier basis. For example, the independence of $A_{\boldsymbol{k}}^j$ and $B_{\boldsymbol{k}}^j$ is a consequence of $\mathrm{Cov}[\cos(\boldsymbol{k}\cdot\boldsymbol{X}_i), \sin(\boldsymbol{k}\cdot\boldsymbol{X}_i)] = 0$. Summation rules for independent normally distributed random variables then reveal that

$$\Omega_{\boldsymbol{k}} = \sum_{j=1}^{J} \frac{\alpha_j^{1/2}}{2^{1/2}} \frac{\Gamma_j}{\Gamma_0} \left(A_{\boldsymbol{k}}^j + i B_{\boldsymbol{k}}^j \right) = \frac{(A_{\boldsymbol{k}} + i B_{\boldsymbol{k}})}{2^{1/2}}, \quad A_{\boldsymbol{k}}, B_{\boldsymbol{k}} \sim \mathcal{N}(0,1). \tag{28}$$

To proceed, consider the random variable $|\Omega_{\boldsymbol{k}}|^2 = \frac{1}{2}(A_{\boldsymbol{k}}^2 + B_{\boldsymbol{k}}^2)$. It is a standard exercise in functions of random variables to show that $|\Omega_{\boldsymbol{k}}|^2 \sim \exp(1)$, where $\exp(\lambda)$ denotes the exponentially distributed random variable with the PDF

$$p(x) = \begin{cases} \lambda e^{-x/\lambda}, & x > 0 \\ 0, & x \leqslant 0. \end{cases} \tag{29}$$

To obtain $W(\varepsilon)$, which is the PDF of $\bar{H}$, it is now a matter of using Eq. (21). Under the uniform ensemble, Eq. (21) expresses $\bar{H}$ as a weighted sum of independent exponential random variables, each of which is shifted to have zero mean. Following EA, the Fourier convolution formula can be used to express the sum as an inverse Fourier transform. The result generalizes that obtained by Pointin and Lundgren [16] [compare their Eq. (41)], namely,

$$W(\varepsilon) = \frac{1}{2\pi} \int_{-\infty}^{\infty} \exp\left\{ i\omega\varepsilon - {\sum_{\boldsymbol{k}}}' \left[\log\left(1 + \frac{i\omega}{(2\pi k)^2} \right) - \frac{i\omega}{(2\pi k)^2} \right] \right\} d\omega, \tag{30}$$

to arbitrary vortex circulations.[2] The integral in (30) can be approximated numerically, however, as with the corresponding expression for bounded domains given by EA [2] [see their Eq. (3.13)], a standard quadrature converges only in the central region where $|\varepsilon| \lesssim 2\sigma_\varepsilon$.

[2]In the work of Pointin and Lundgren [16], (30) is obtained by the method of moments and is valid for unit vortex circulations (± 1) only.

An alternative and more explicit result, with much better convergence properties in the positive tail region ($\varepsilon \gtrsim 2\sigma_\varepsilon$), can be obtained using Laplace transforms. In Appendix C 1, an explicit formula for the weighted sum of a finite number of exponential random variables is derived, building on previous results in the literature [28]. For the case of an infinite sum, as in (21), a means of truncating the sum so that it converges rapidly is described in Appendix C 2. Applying these results to (21), the following exact (formal) formula is obtained:

$$W(\varepsilon) = \lim_{k_m \to \infty} \sum_{k<k_m} \sum_{j=1}^{q_k} C_{k,k_m}^{q_k - j} g_j(\varepsilon + \varepsilon_m, 4\pi^2 k^2), \tag{31}$$

where

$$g_j(x,\lambda) = \frac{\lambda^j x^{j-1}}{(j-1)!} e^{-\lambda x} \quad (x > 0) \tag{32}$$

is the PDF of the Erlang distribution (Gamma distribution with integer index). The sum over k is taken over all unique values of $k = |\boldsymbol{k}|$ encountered in the primed sum defined in (5), satisfying $k < k_m$ (a maximum wave number). For example, the first ten values of k in the sum are $\{1, \sqrt{2}, 2, \sqrt{5}, \sqrt{8}, 3, \sqrt{10}, \sqrt{13}, 4, \sqrt{17}, \ldots\}$. The integers $\{q_k\}$ denote the multiplicity of each wave-number amplitude (i.e., number of wave numbers $\boldsymbol{k}$ with $|\boldsymbol{k}| = k$), with the first ten values of q_k being $\{2,2,2,4,2,2,4,4,2,4, \ldots\}$. Notice that, due to the symmetries of the wave-number lattice, q_k increases unboundedly. Finally, the constants ε_m and C_{k,k_m}^j are given by

$$\begin{aligned}
\varepsilon_m &= \sum_{k<k_m} \frac{q_k}{4\pi^2 k^2}, \\
C_{k,k_m}^j &= \frac{(-1)^j}{j!} a_{k,k_m} B_j\left(c_{k,k_m}^1, c_{k,k_m}^2, \ldots, c_{k,k_m}^j\right), \\
a_{k,k_m} &= \prod_{k'<k_m, k' \neq k} \left(\frac{k'^2}{k'^2 - k^2}\right)^{q_{k'}}, \\
c_{k,k_m}^i &= (i-1)! \sum_{k'<k_m, k' \neq k} \frac{q'_k k^{2i}}{(k'^2 - k^2)^i}.
\end{aligned} \tag{33}$$

The $B_j(x_1, \ldots, x_j)$ function in (33) denotes the complete Bell polynomials (see Appendix C 1 for discussion).

Formulas (31)–(33), although formally exact, are unfortunately impractical for calculations. As k_m is increased, ε_m increases unboundedly and the absolute value of the coefficients C_{k,k_m}^j also increase rapidly with k_m. The nature of cancellations between terms in the formula means that high precision computer arithmetic is necessary to evaluate $W(\varepsilon)$ accurately, even for a truncation as low as $k_m = 8.5$ (eight wave-number shells). An approximation is required for a practical formula.

Fortunately, a relatively simple approximation can be found, as described in Appendix C 2 below. Equation (31) is approximated by

$$W(\varepsilon; k_m) = \sum_{k<k_m} \sum_{j=1}^{q_k} C_{k,k_m}^{q_k - j} F_j\left(\varepsilon + \varepsilon_m, k^2, \sigma_m^2\right). \tag{34}$$

The formula (34) is identical to a truncation of (31), except that the Erlang PDFs g_j have been replaced by the PDFs F_j. Here $F_j(x,\lambda,\sigma^2)$ denotes the PDF of a random variable generated by a convolution between the Erlang distribution with PDF $g_j(x,\lambda)$ and a normal random variable with zero mean and variance σ^2. An explicit formula for F_j is given in Appendix C 2. Finally, the variance used in (34) is $\sigma_m^2 = \sum_{k \geqslant k_m} q_k/(2\pi k)^4$.

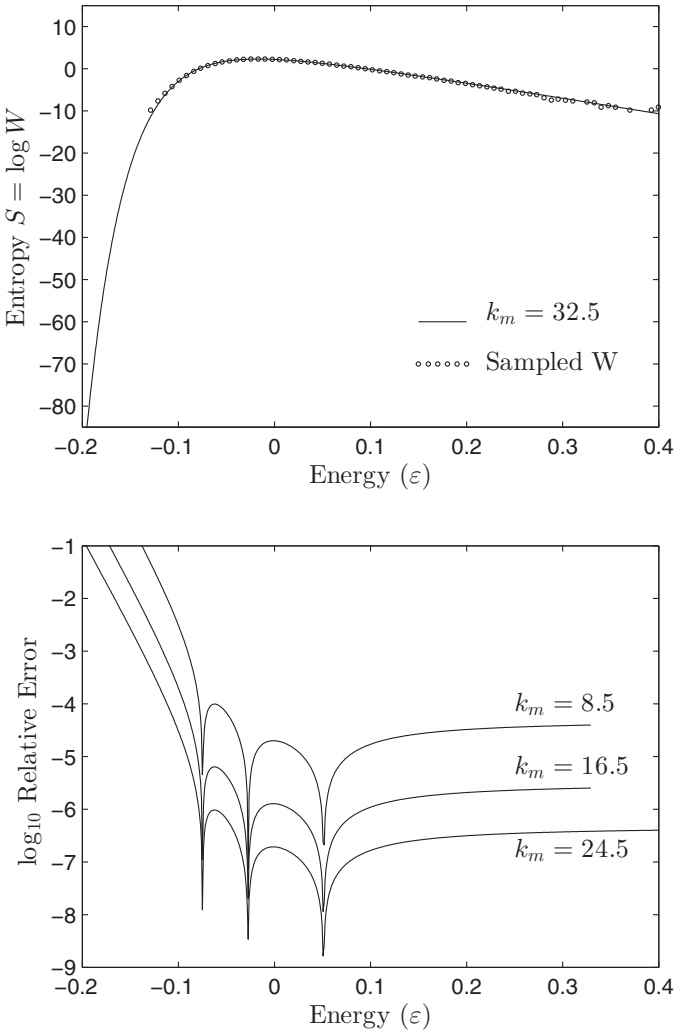

FIG. 6. Shown on top is the entropy $S(\varepsilon) = \log W(\varepsilon)$ as a function of vortex interaction energy ε. The solid black curve shows the $N \to \infty$ analytical result from Eq. (34) truncated at $k_m = 32.5$ and the dotted curve is calculated from statistical sampling of the microcanonical ensemble with $N = 50$. The bottom shows the relative truncation error in Eq. (34), measured with respect to the $k_m = 32.5$ calculation, when $k_m = 8.5$, 16.5, and 24.5.

The formula (34), although rather complicated, is reasonably straightforward to evaluate numerically using standard routines for Bell and Hermite polynomials. The nature of cancellations in the formula remains such that variable precision arithmetic must be used to evaluate the coefficients C^j_{k,k_m}. However, these coefficients are properties of the wave-number lattice alone and do not depend on the distribution of vortex circulations. Hence they need only be calculated once (i.e., once for each truncation wave number k_m). Figure 6 (top panel) plots the entropy $S(\varepsilon) = \log W(\varepsilon)$ calculated using (34) with truncation wave number $k_m = 32.5$. The result is compared with that from a histogram generated by a direct statistical sampling of $\bar{H}$ with $N = 50$ uniformly distributed vortices (10^7 samples are used).

To give an idea of the rate of convergence of (34) as k_m is increased, Fig. 6 (bottom panel) plots the relative error in $W(\varepsilon)$ for a range of values of the truncation wave number k_m, relative to the

highest value used ($k_m = 32.5$). Convergence is evidently relatively rapid in the central region. By comparison, however, it is necessary to use a relatively high value of k_m to accurately evaluate $W(\varepsilon)$ in the tails, particularly the left tail (dipole forming regime).

B. Equilibrium energy spectrum

The density of states function $W(\varepsilon)$ encodes all the information necessary to determine the equilibrium energy spectrum of point vortex turbulence (see [2] for the case of bounded domains). In the doubly periodic domain the main result can be obtained relatively straightforwardly.

The starting point is to consider the microcanonical PDF $p_\varepsilon(e_k)$ for the distribution of energy $E_{\boldsymbol{k}} = |\Omega_{\boldsymbol{k}}|^2/4\pi^2k^2$ in a Fourier mode $\boldsymbol{k}$ with total wave number $k = |\boldsymbol{k}|$. In terms of the uniform distribution defined above, the microcanonical PDF $p_\varepsilon(e_k)$ can be interpreted as the PDF of the conditional random variable $E_{\boldsymbol{k}}|\bar{H} = \varepsilon$. Consequently, Bayes's theorem in the form

$$\mathbb{P}(E_{\boldsymbol{k}}|\bar{H}) = \frac{\mathbb{P}(\bar{H}|E_{\boldsymbol{k}})\,\mathbb{P}(E_{\boldsymbol{k}})}{\mathbb{P}(\bar{H})}$$

can be used to express $p_\varepsilon(e_k)$ in terms of calculable quantities as

$$p_\varepsilon(e_k) = \frac{W_{-\boldsymbol{k}}(\varepsilon + e_{0k} - e_k)p_0(e_k)}{W(\varepsilon)}. \tag{35}$$

Here $W_{-\boldsymbol{k}}(\cdot)$ denotes the density of states function (31) evaluated with wave number $\boldsymbol{k}$ omitted from the calculation. The $W_{-\boldsymbol{k}}$ term in (35) is the conditional PDF for $\bar{H}$ given that $E_{\boldsymbol{k}} = e_k$. The PDF of $E_{\boldsymbol{k}}$ under the uniform ensemble is denoted by $p_0(e_k)$ and from (29) is given by

$$p_0(e_k) = 4\pi^2k^2e^{-4\pi^2k^2e_k} \quad (e_k > 0); \tag{36}$$

the constant $e_{0k} = (2\pi k)^{-2}$ is the mean of this distribution.

Under the ergodic hypothesis, $p_\varepsilon(e_k)$ is also the long-time PDF of $E_{\boldsymbol{k}}$ in a dynamical run with $\bar{H} = \varepsilon$. The fact that the microcanonical ensemble is restricted to a hypersurface with constant $\bar{H}$ means that $p_\varepsilon(e_k)$ can differ significantly from the exponentially distributed $p_0(e_k)$, as will be discussed below. The expected value of $E_{\boldsymbol{k}}$, which defines the equilibrium energy spectrum, is

$$\langle E_{\boldsymbol{k}}\rangle = \int_0^\infty e_k p_\varepsilon(e_k)de_k = \frac{4\pi^2k^2}{W(\varepsilon)}\int_0^\infty e_k W_{-\boldsymbol{k}}(\varepsilon + e_{0k} - e_k)e^{-4\pi^2k^2e_k}de_k. \tag{37}$$

The convolution result

$$(p_0 * p_0)(e_k) = 4\pi^2k^2e_k p_0(e_k)$$

can be used to express (37) as a convolution

$$\langle E_{\boldsymbol{k}}\rangle = \frac{(p_0 * p_0 * W_{-\boldsymbol{k}})(\varepsilon + e_{0k})}{4\pi^2k^2W(\varepsilon)},$$

which can be further simplified by noting, from the fact that $p_\varepsilon(e_k)$ is a PDF and thus has unit integral, that

$$W(\varepsilon) = (p_0 * W_{-\boldsymbol{k}})(\varepsilon + e_{0k}),$$

to give

$$\langle E_{\boldsymbol{k}}\rangle = \frac{(p_0 * W)(\varepsilon)}{4\pi^2k^2W(\varepsilon)} = \frac{1}{W(\varepsilon)}\int_0^\infty W(\varepsilon - e_k)e^{-4\pi^2k^2e_k}de_k. \tag{38}$$

Equation (38) is significant because it confirms that all of the information about the energy spectrum is encoded in the density of states function $W(\varepsilon)$. Equation (38) differs from an equivalent result for bounded domains in the work of EA [2] (see their Sec. 3.3) by a factor of 2, which is accounted for by the natural degeneracy of all eigenfunctions in the doubly periodic domain. (In the notation

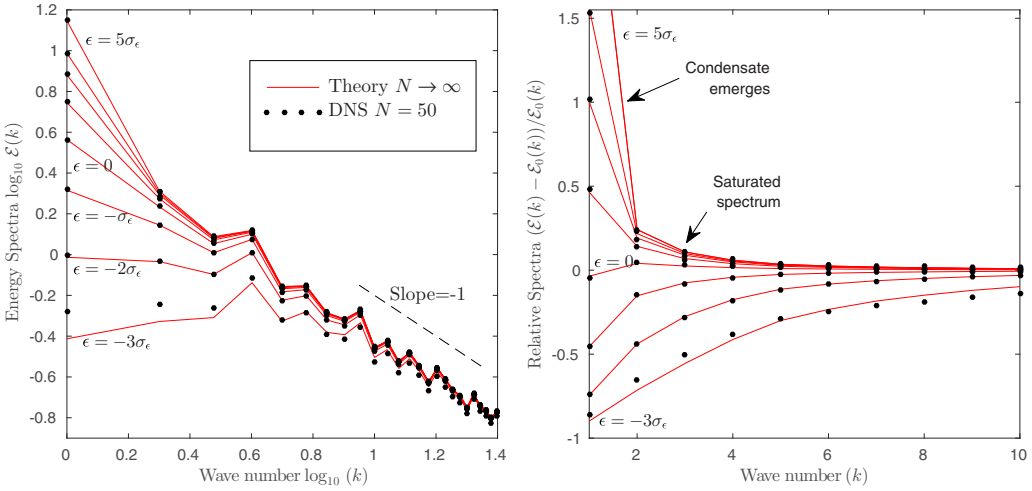

FIG. 7. Shown on the left is the energy spectrum $\log_{10}\mathcal{E}(k)$ calculated from Eq. (38) (solid curves) and from the $N=50$ DNS long-time averages (dotted curves with symbols). The DNS with VIE $\varepsilon=-3\sigma_\varepsilon$, $-2\sigma_\varepsilon$, $-\sigma_\varepsilon$, 0, σ_ε, $2\sigma_\varepsilon$, $3\sigma_\varepsilon$, and $5\sigma_\varepsilon$ is shown. On the right are the relative energy spectra for the same DNS $[\mathcal{E}(k)-\mathcal{E}_0(k)]/\mathcal{E}_0(k)$ measured with respect to the randomized spectrum $\mathcal{E}_0(k)$ [plotted as a function of k as opposed to $\log_{10}(k)$].

of [2], the domain inverse temperatures of the doubly periodic domain are $\beta_k=-4\pi^2k^2$ and each has multiplicity $2q_k$.) Formulas for higher moments of the energy in each mode $\langle(E_{\boldsymbol{k}})^q\rangle$ can be obtained using a similar method.

C. Comparison with $N=50$ simulations

The results of Sec. IV B can be tested by comparison with long-time statistics obtained from DNS. Comparison with direct statistical sampling of the microcanonical ensemble in [2] indicates that, at least in bounded domains, the $N\to\infty$ statistical results can be reasonably accurate for as few as $N=20$–100 vortices. Consequently, statistics from the $N=50$ DNS described in Sec. III A will be used here to verify the theory.

In Fig. 7 energy spectra obtained from the DNS are compared with those predicted by Eq. (38). In practice, $W(\varepsilon)$ is calculated on a well-resolved grid using (34) and numerical quadrature is then used to evaluate (38). An alternative approach would be to integrate (38) explicitly to obtain analytical formulae, however such an approach is unwieldy, as well as being computationally expensive to evaluate for all possible $\boldsymbol{k}$. In Fig. 7, as is standard in the turbulence literature, the energy spectra $\mathcal{E}(k)$ are presented as functions of the total wave number $k=|\boldsymbol{k}|$. For simplicity and reproducibility $\mathcal{E}(k)$ are obtained from the discretized energy in each Fourier mode $E_{\boldsymbol{k}}$ by summation over wave-number shells

$$\mathcal{E}(k)=\sum_k{}' E_{\boldsymbol{k}}, \tag{39}$$

where the subscript k on the summation denotes that the sum is over all wave numbers (in the primed summation defined above) with $k-\frac{1}{2}\leqslant|\boldsymbol{k}|<k+\frac{1}{2}$. Notice that the $\mathcal{E}(k)$ curves appear rough at low wave numbers due to variations in the number of wave numbers per shell.

Figure 7 shows excellent agreement between the spectra $\mathcal{E}(k)$ calculated from the DNS (dotted curves with symbols) and those obtained from Eq. (38) (solid curves). The agreement holds across a wide range of VIE, from $\varepsilon=-2\sigma_\varepsilon$ to $5\sigma_\varepsilon$. Whereas the left panel shows the spectra as a function of $\log_{10}k$, the right panel shows the relative spectra, measured with respect to the randomized spectra $\mathcal{E}^0(k)$ (see Sec. II C above) as a function of k. The relative spectra reveal that there is a strong asymmetry in the organization of the system depending on whether ε is positive or negative. At

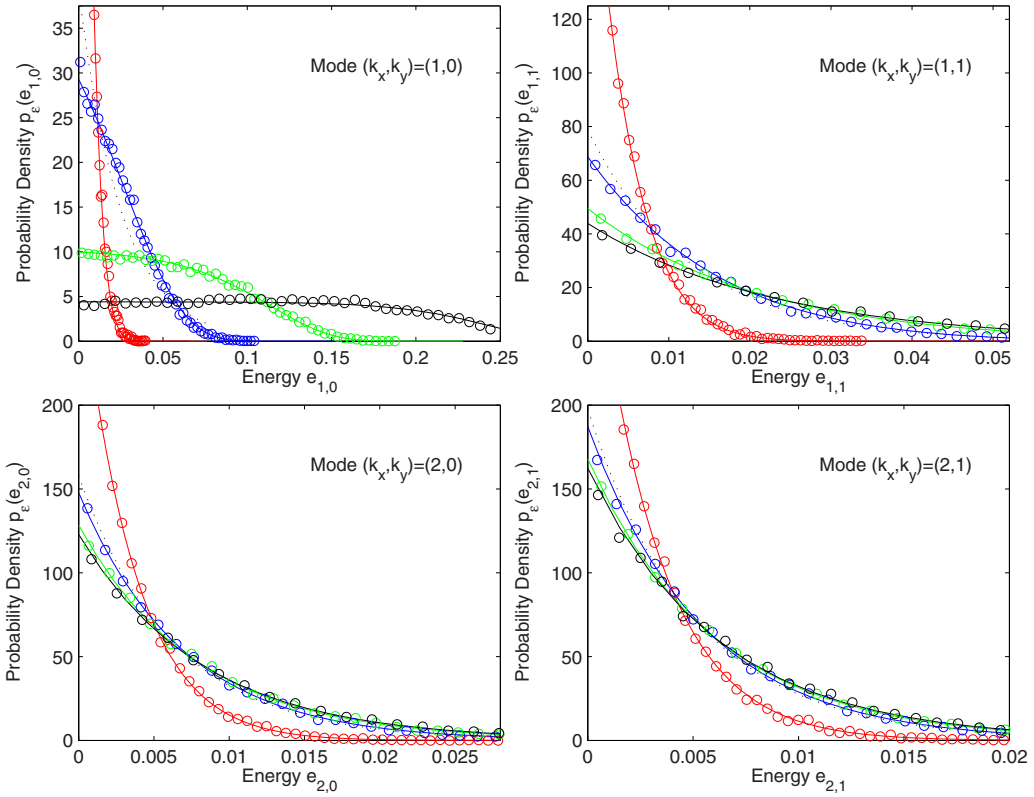

FIG. 8. Microcanonical PDF $p_\varepsilon(e_{\boldsymbol{k}})$ of the energy $E_{\boldsymbol{k}}$ in the Fourier mode with wave number $\boldsymbol{k}$, (i) calculated from Eq. (35) (solid curves) and (ii) calculated from DNS long-time statistics (open circles): top left, $\boldsymbol{k} = (1,0)^T$; top right, $\boldsymbol{k} = (1,1)^T$; bottom left, $\boldsymbol{k} = (2,0)^T$; and bottom right, $\boldsymbol{k} = (2,1)^T$. Results are given for four VIE levels (corresponding to DNS) $\varepsilon = -2\sigma_\varepsilon$, 0, $2\sigma_\varepsilon$, and $5\sigma_\varepsilon$ (red, blue, green and black curves respectively). The dotted line on each panel shows the PDF $p_0(e_{\boldsymbol{k}})$ of $E_{\boldsymbol{k}}$ under the uniform distribution (randomized vortices).

negative ε the energy deficit in the spectrum, compared to the randomized spectrum, is spread over a significant range of wave numbers and decays smoothly with increasing k. At positive ε, by contrast, the energy surplus in the spectrum is concentrated almost entirely in the gravest ($k = 1$) Fourier modes, consistent with the emergence of the Onsager-Kraichnan condensate [9,10]. For $k > 1$ the spectrum is saturated. An asymptotic treatment of the $\varepsilon \to \infty$ limit in Appendix D reveals that the saturated spectrum is given by

$$\lim_{\varepsilon\to\infty} \langle E_{\boldsymbol{k}} \rangle = \frac{1}{4\pi^2(k^2-1)} \quad (k > 1), \tag{40}$$

which can be compared with the randomized spectrum $\langle E_{\boldsymbol{k}} \rangle_0 = 1/4\pi^2 k^2$. The condensate modes $\boldsymbol{k} = (0,1)^T$ and $(1,0)^T$ contain the remaining excess energy [see Eq. (D4)].

Significantly poorer agreement between theory and DNS is found for strongly negative VIE, e.g., $\varepsilon = -3\sigma_\varepsilon$. The dynamics at negative VIE is governed by dipoles with progressively smaller separation scales. The poor agreement with the statistical theory may be due to either the time scale for ergodicity being greatly increased in the DNS or an increased sensitivity to finite N (vortex number) in the dipole regime. A different statistical theory, which explicitly takes account of dipole formation, may be more successful in this regime.

In Fig. 8 the microcanonical PDFs $p_\varepsilon(e_k)$ given by Eq. (35) (solid curves), for the energy $E_{\boldsymbol{k}}$ in the Fourier mode $\boldsymbol{k}$, are compared with statistics compiled from the $N = 50$ integrations (open

circles). Fourier modes with total wave number $k = 1, \sqrt{2}, 2$, and $\sqrt{5}$ are shown and the comparison is for four different VIE $\varepsilon = -2\sigma_\varepsilon$, 0, $2\sigma_\varepsilon$, and $5\sigma_\varepsilon$. For comparison, the exponential distribution $p_0(e_k)$ [Eq. (36)] of $E_{\boldsymbol{k}}$ under the uniform ensemble (vortices positioned at random) is given by the dotted line in each panel. The formula (35) is seen in Fig. 8 to capture the PDF of $E_{\boldsymbol{k}}$ in the integrations with good accuracy. Unsurprisingly, it is the gravest ($k = 1$) mode that shows the greatest departure from the exponential distribution, with greatly increased probability of finding high energies at large positive ε compared with significantly reduced probability of even moderate energies at negative ε. Naturally, this outcome is consistent with the snapshots of Fig. 2, as the dipole-dominated configuration at $\varepsilon = -2\sigma_\varepsilon$ will tend to project only very weakly onto the Fourier modes with $k = 1$. By contrast the like-signed clusters evident at $\varepsilon = 5\sigma_\varepsilon$ will project strongly onto the $k = 1$ modes.

There is additional evidence of spectral saturation in Fig. 8, as the PDFs $p_\varepsilon(e_k)$ at positive VIE ($\varepsilon = 2\sigma_\varepsilon$ and $5\sigma_\varepsilon$) are very similar for $k > 1$. In fact, the limiting distributions can be deduced from (35) using (D4), from which it can be deduced that $W(\varepsilon) \sim \varepsilon e^{-4\pi^2\varepsilon}$ and (by the same arguments) $W_{-\boldsymbol{k}}(\varepsilon) \sim \varepsilon e^{-4\pi^2\varepsilon}$ provided $k > 1$. Examining the limiting behavior of (35), it follows that

$$\lim_{\varepsilon\to\infty} p_\varepsilon(e_k) = 4\pi^2(k^2-1)e^{-4\pi^2(k^2-1)e_k} \quad (e_k > 0), \tag{41}$$

which corresponds closely to the $\varepsilon = 5\sigma_\varepsilon$ curves plotted in Fig. 8. In other words, as $\varepsilon \to \infty$ the energy in the saturated Fourier modes with $k > 1$ is exponentially distributed, but with a mean value greater than that expected from the uniform distribution (36). It is to be emphasized that this limiting behavior does not apply to the condensate ($k = 1$) modes, which are not exponentially distributed as $\varepsilon \to \infty$.

V. CONCLUSION

In this work the point vortex system in the doubly periodic domain $\mathcal{D}$ has been shown to have the following characteristics.

(i) It exhibits no evidence of nonergodic behavior (for $N \geqslant 6$), contradicting the earlier conclusion of WM [17]. A significant question mark surrounding the validity of the methods of equilibrium statistical mechanics applied to the point vortex system has therefore been removed. In fact, our conclusion is further supported by recent numerical studies with $N \sim 10^2$ in both conformal bounded domains [2] and on the sphere [1]. These studies compared DNS time averages and microcanonical averages and also found no evidence of nonergodicity, in common with earlier studies in polygonal domains [29]. It is to be emphasized, however, that our results do not constitute a proof of ergodicity; the system is in fact nonergodic at large VIE [20]. Nevertheless, our results and the other numerical studies cited above suggest that, for the practical application of statistical mechanics at moderate values of the VIE, the hypothesis of ergodicity appears to be a reasonable working assumption for $N \geqslant 6$.

(ii) The point vortex system has statistics that are independent of the initial value of the vortex momentum $\boldsymbol{P}$ in the limit $N \to \infty$, in the case of irrational vortex circulation ratios, or indeed for continuous vorticity distributions. The vortex momentum, which arises as a conserved quantity in $\mathcal{D}$ because of continuous symmetries in the x and y directions, therefore need not be accounted for in statistical treatments, including notably the Miller-Robert-Sommeria (MRS) statistics [30,31]. Under a suitable hypothesis of ergodicity, the MRS statistics extend the Joyce-Montgomery [14] mean field theory for point vortices to continuous initial vorticity profiles and have been used to predict the end states of decaying 2DCT flows [32].

(iii) The system has solvable statistics in the limit $N \to \infty$, in the sense that the density of states function $W(\varepsilon)$ can be obtained analytically [Eq. (31)], and the equilibrium energy spectrum can be obtained from $W(\varepsilon)$ [cf. Eq. (38)]. The statistics are largely independent of the distribution of vortex circulations $\boldsymbol{\Gamma}$ except for a scaling factor involving the rms circulation Γ_0. Both ergodicity [(i) above] and the justified neglect of $\boldsymbol{P}$ [(ii) above] are necessary conditions for the treatment given here, which extends the results of EA [2] to the doubly periodic domain. The results have

been verified by comparison with time-averaged statistics taken from DNS with $N = 50$ (see Figs. 7 and 8).

The results presented above will be of interest for the interpretation of statistics of 2DCT and 2DQT. For both systems, the regime in which the point vortex model is most relevant is the dilute regime discussed in the Introduction, in which the spatial density of vortices is sufficiently low that nonequilibrium processes such as like-sign vortex merger (in 2DCT) and opposite-sign annihilation (in 2DQT) are relatively infrequent. Evidence that the dilute regime is relevant in practice is provided by the recent numerical simulations of 2DQT in the Gross-Pitaevskii (defocusing nonlinear Schrödinger) equations by Billam *et al.* [9]. The low-wave-number part of the incompressible energy spectrum was found to correspond closely to that of the point vortex system across a range of values of the VIE ε, in simulations where the "healing length" is small compared to the domain. Whether a similar regime exists for 2DCT is left for future work. In particular, it will be interesting to examine the extent to which an empirical model of vortex population evolution [8] or an explicit kinetic theory of vortex merger events [6] can be combined with the present theory to predict the time evolution of the energy spectrum.

Overall our results should be reassuring for researchers using the doubly periodic domain $\mathcal{D}$ for numerical simulations of turbulence. In particular, neglecting $\boldsymbol{P}$ is justified in most theoretical treatments. The influence of $\boldsymbol{P}$ is significant only when a small number of vortices with quantized circulation are present. However, even in the case with $N = 6$ considered here the effect is small, as the maximum influence of $\boldsymbol{P}$ on the dynamics is comparable to that of a relatively modest change in the VIE ($\approx 0.5\sigma_\varepsilon$). Nevertheless, it should be emphasized that the role of the domain geometry is always important in point vortex dynamics and two-dimensional fluid dynamics in general, because of the nature of long-range interactions in the system. Compared to bounded domains, studied by EA [2], $\mathcal{D}$ retains some peculiar features. One of the main results of [2] was that geometry, through the distribution of eigenvalues of the hydrodynamic eigenvalue problem, has a strong influence on the nature of the Onsager-Kraichnan condensation in the point vortex system. Viewed from this perspective $\mathcal{D}$ is an extreme outlier in that the lead eigenvalue (corresponding to Fourier modes with $k = |\boldsymbol{k}| = 1$) has a fourfold degeneracy [each wave number $\boldsymbol{k}$ has a twofold degeneracy and $\boldsymbol{k} = (0,1)^T$ and $(1,0)^T$ each have $k = 1$]. The consequence of this degeneracy is that, compared to a bounded domain, the condensate has four times the degrees of freedom across which to share its energy. As a result, coherent structures will emerge in $\mathcal{D}$ at significantly higher VIE compared to the bounded case.

ACKNOWLEDGMENTS

J.G.E. would like to acknowledge the hospitality of the Kavli Institute for Theoretical Physics, where this research was supported in part by the National Science Foundation under Grant No. NSF PHY11-25915. Tom Ashbee is thanked for helpful comments.

APPENDIX A: DISTRIBUTIONS OF VORTEX IMPULSE

The distribution of P_x when the $N = 6$ vortices are distributed randomly in $\mathcal{D}$ is plotted in Fig. 1 (top panel). The PDF of the distribution of P_x for N vortices with $\Gamma_i = \pm 1$ can be obtained explicitly from the following formula for the PDF of the sum of N independent and identically distributed random variables:

$$p_N(x) = (2\pi)^{(N-1)/2} \int_{-\infty}^{\infty} \hat{p}(k)^N e^{ikx} dk, \quad \hat{p}(k) = \frac{1}{\sqrt{2\pi}} \int_{-\infty}^{\infty} p(x) e^{-ikx} dx.$$

Here

$$p(x) = \frac{1}{2\pi} \begin{cases} 1, & |x| \leqslant \pi \\ 0, & |x| > \pi \end{cases}$$

is the uniform distribution. For $N = 6$ the result is

$$p_6(x) = \frac{1}{15 \times 2^{10}\pi^6}(|x-6\pi|^5 - 6|x-4\pi|^5 + 15|x-2\pi|^5 - 20|x|^5 + 15|x+2\pi|^5 - 6|x+4\pi|^4 + |x+6\pi|^5). \tag{A1}$$

For the $N = 50$ case plotted in Fig. 1 (bottom panel) the central limit theorem approximation is used

$$p_N(x) \approx \frac{1}{(2\pi N)^{1/2}\sigma} \exp\left(-\frac{x^2}{2\sigma^2 N}\right), \quad \sigma^2 = \frac{\pi^2}{3}.$$

APPENDIX B: GREEN'S FUNCTION DETAILS

To preserve the link between the Navier-Stokes equations (1) and the point vortex system (9) it is helpful to use precisely the same Green's function $G(\boldsymbol{x},\boldsymbol{x}')$ in each case. An arbitrary constant can be added to $G(\boldsymbol{x},\boldsymbol{x}')$ without changing the point vortex equations of motion and $G(\boldsymbol{x},\boldsymbol{x}')$ can be multiplied by an arbitrary factor provided time is rescaled in (9), again without loss of generality. Since they were concerned solely with point vortices, WM used both devices. It may therefore be helpful to researchers to have a record of the form of $G(\boldsymbol{x},\boldsymbol{x}')$, consistent with WM's formulation, which is exactly equal to (3). The form is

$$G(\boldsymbol{x},\boldsymbol{x}') = \frac{1}{4\pi}\left[\sum_{m=-\infty}^{\infty} \log\left(\frac{\cosh(x-x'-2\pi m) - \cos(y-y')}{\cosh 2\pi m}\right) - \frac{(x-x')^2}{2\pi} - G_{00}\right]. \tag{B1}$$

The constant G_{00} must be chosen so that

$$\int_{\mathcal{D}^2} G(\boldsymbol{x},\boldsymbol{x}')d\boldsymbol{x}\,d\boldsymbol{x}' = 0$$

for consistency with (3). Derivatives of (B1), which are needed to integrate the equations of motion (9), are obtained following Sec. II of [17].

To evaluate G_{00} we use the following:

$$\begin{aligned}
G_{00} &= \frac{1}{(4\pi^2)^2}\int_{\mathcal{D}^2}\left[\sum_{m=-\infty}^{\infty} \log\left(\frac{\cosh(x-x'-2\pi m) - \cos(y-y')}{\cosh 2\pi m}\right) - \frac{x^2}{2\pi}\right]d\boldsymbol{x}\,d\boldsymbol{x}' \\
&= \frac{1}{4\pi^2}\int_0^{2\pi}\int_0^{2\pi}\left\{\sum_{m=-\infty}^{\infty}\left[\log\left(\frac{\cosh(x-2\pi m) - \cos(y)}{\cosh 2\pi m}\right)\right] - \frac{x^2}{2\pi}\right\}dy\,dx \\
&= \frac{1}{2\pi}\int_0^{2\pi}\left\{\sum_{m=-\infty}^{\infty}\left[\log\left(\frac{\exp|x-2\pi m|}{2}\right) - \log(\cosh 2\pi m)\right] - \frac{x^2}{2\pi}\right\}dx \\
&= \frac{1}{2\pi}\int_0^{2\pi}\left[\sum_{m=1}^{\infty} 2\Big(2\pi m - \log(2\cosh 2\pi m)\Big) + x - \log 2 - \frac{x^2}{2\pi}\right]dx \\
&= \frac{\pi}{3} - \log 2 - 2\sum_{m=1}^{\infty}\log(1+e^{-4\pi m}) \approx 0.354\,043\,4.
\end{aligned}$$

This value has been confirmed to be correct by numerical evaluation of (3) and (B1).

APPENDIX C: SUMMATION OF EXPONENTIAL RANDOM VARIABLES

In this Appendix we give details of the procedure used to evaluate the density of states formula (31). First an exact and practical analytical formula for the PDF of a weighted sum of

M independent and identically distributed exponential random variables is given. Second, the case of numerical evaluation for $M \to \infty$ is discussed, because in this case the exact formula involves infinite sums and products that necessitate a suitable truncation.

1. Analytical formula for finite M

Let $p_{\boldsymbol{w}}(x)$ denote the PDF of the weighted sum S_M of M independent and identically distributed exponential random variables $\{X_m\}$, each with PDF $p(x) = \mathrm{e}^{-x} H(x)$, where $H(x)$ is the Heaviside step function. Here $\boldsymbol{w} = (w_1, w_2, w_3, \ldots)^T$ denotes a (possibly infinite) vector of M nondecreasing real constants and the weighted sum in question is

$$S_M = \sum_{m=1}^{M} \frac{X_m}{w_m}.$$

The aim here is to obtain an exact formula for $p_{\boldsymbol{w}}(x)$ when M is finite. A previous formula [28] has appeared in the literature, but compared to the present result it is unwieldy for calculations. The limit with $M \to \infty$ is discussed in the following section.

Note first that the PDF $p_{\boldsymbol{w}}(x)$ of S_M can be written as a convolution

$$p_{\boldsymbol{w}}(x) = (p_1 * p_2 * \cdots * p_M)(x),$$

where $p_m(x) = w_m e^{-w_m x} H(x)$ is the PDF of X_m/w_m. Taking Laplace transforms,

$$\bar{p}_{\boldsymbol{w}}(s) = \bar{p}_1(s)\bar{p}_2(s)\cdots\bar{p}_M(s) = \prod_{m=1}^{M} \frac{w_m}{s + w_m}.$$

In the simplest case, where the $\{w_i\}$ are distinct, an explicit formula can be obtained directly as a sum of residues, using the Cauchy residue theorem with the Bromwich integral, giving (for $x > 0$)

$$p_{\boldsymbol{w}}(x) = \sum_{m=1}^{M} \mathrm{Res}\left(\frac{w_1 w_2 \cdots w_M e^{xs}}{(s + w_1)(s + w_2)\cdots(s + w_M)}; s = -w_m \right) = \sum_{m=1}^{M} A_m w_m e^{-w_m x}, \tag{C1}$$

where

$$A_m = \prod_{i=1, w_i \neq w_m}^{M} \frac{w_i}{w_i - w_m}.$$

It is clear, however, that the formula (C1) fails whenever $w_i - w_m = 0$ for any $i \neq m$. The general result can be obtained as follows. Define $\{W_1, \ldots, W_K\}$ to be the K unique ($K \leqslant M$) values of the $\{w_m\}$, with multiplicities $\{q_1, \ldots, q_K\}$ (so that $\sum_{k=1}^{K} q_k = M$). The Bromwich formula is then

$$p_{\boldsymbol{w}}(x) = \sum_{k=1}^{K} \mathrm{Res}\left(\frac{W_1^{q_1} W_2^{q_2} \cdots W_K^{q_K} e^{xs}}{(s + W_1)^{q_1}(s + W_2)^{q_2} \cdots (s + W_K)^{q_K}}; s = -W_k \right)$$

or, exploiting the fact that partial derivatives commute with the residue formula,

$$p_{\boldsymbol{w}}(x) = \frac{(-1)^{M-K} W_1^{q_1} W_2^{q_2} \cdots W_K^{q_K}}{(q_1 - 1)!(q_2 - 1)! \cdots (q_K - 1)!} \left(\frac{\partial}{\partial W_1} \right)^{q_1 - 1} \left(\frac{\partial}{\partial W_2} \right)^{q_2 - 1} \cdots \left(\frac{\partial}{\partial W_K} \right)^{q_K - 1}$$
$$\times \sum_{k=1}^{K} \mathrm{Res}\left(\frac{e^{xs}}{(s + W_1)(s + W_2)\cdots(s + W_K)}; s = -W_k \right). \tag{C2}$$

TABLE I. First few complete Bell polynomials.

B_0	1
$B_1(x_1)$	x_1
$B_2(x_1,x_2)$	$x_2 + x_1^2$
$B_3(x_1,x_2,x_3)$	$x_3 + 3x_2x_1 + x_1^3$
$B_4(x_1,x_2,x_3,x_4)$	$x_4 + 4x_3x_1 + 3x_2^2 + 6x_2x_1^2 + x_1^4$
$B_5(x_1,x_2,x_3,x_4,x_5)$	$x_5 + 5x_4x_1 + 10x_3x_2 + 10x_3x_1^2 + 15x_2^2x_1 + 10x_2x_1^3 + x_1^5$
$B_6(x_1,x_2,x_3,x_4,x_5,x_6)$	$x_6 + 6x_5x_1 + 15x_4x_2 + 15x_4x_1^2 + 10x_3^2 + 60x_3x_2x_1$
	$\cdots + 20x_3x_1^3 + 15x_2^3 + 45x_2^2x_1^2 + 15x_2x_1^4 + x_1^6$

Evaluating the residues as above and differentiating with respect to each variable except W_k, (C2) simplifies (when $x > 0$) to

$$p_{\boldsymbol{w}}(x) = \sum_{k=1}^{K} \frac{(-1)^{q_k-1} W_k^{q_k}}{(q_k-1)!} \left(\frac{\partial}{\partial W_k}\right)^{q_k-1} [A_k(W_k) e^{-W_k x}]$$
$$= \sum_{k=1}^{K} \frac{W_k^{q_k}}{(q_k-1)!} \sum_{j=0}^{q_k-1} \binom{q_k-1}{j} (-1)^j x^{q_k-1-j} e^{-W_k x} A_k^{(j)}(W_k). \tag{C3}$$

Here

$$A_k(W_k) = \prod_{i=1, w_i \neq W_k}^{M} \frac{w_i}{w_i - W_k}$$

is defined exactly as A_m in (C1) above, except that here the product is over $M - q_k$ terms as opposed to $M - 1$ terms in the former case. The jth derivative of $A_k(W_k)$, which appears in (C3), can be evaluated by first writing $A_k(W_k)$ as an exponential

$$A_k(W_k) = \exp\left(\sum_{i=1, w_i \neq W_k}^{M} \log w_i - \log|w_i - W_k| \right)$$

and then using Faà di Bruno's formula for differentiation of the exponential of a function

$$\left(\frac{d}{dx}\right)^j e^{f(x)} = B_j(f', f'', \ldots, f^{(j)}) e^{f(x)},$$

where $B_j(x_1, \ldots, x_j)$ is the (exponential) complete Bell polynomial of order j (by convention $B_0 = 1$). The complete Bell polynomials are familiar from introductory statistics because they express the moments of a random variable in terms of its cumulants and they satisfy recursive formulas allowing for straightforward evaluation. The first six are given in Table I.

Applying Faà di Bruno's formula, the result is

$$A_k^{(j)}(W_k) = \frac{B_j(C_1^k, C_2^k, \ldots, C_j^k)}{W_k^j} A_k(W_k), \quad C_j^k = \sum_{i=1,\, w_i \neq W_k}^{M} \frac{(j-1)!\, W_k^j}{(w_i - W_k)^j}.$$

Inserting this above and reindexing gives

$$p_{\boldsymbol{w}}(x) = \sum_{k=1}^{K} \sum_{j=1}^{q_k} \frac{(-1)^{q_k-j} B_{q_k-j}\left(C_1^k, C_2^k, \ldots, C_{q_k-j}^k\right) A_k}{(q_k-j)!} \frac{W_k^j}{(j-1)!} x^{j-1} e^{-W_k x}. \tag{C4}$$

The formula (C4) scales efficiently for calculations. In fact, given a standard recursive routine for evaluating the Bell polynomials, at fixed M it requires a comparable number of operations to (C2) (notice that the total number of constants $\{C_j^k\}$ and $\{A_k\}$ requiring evaluation is exactly M in both cases).

The result (C4) can be recognized as a sum of Erlang distributions. Two useful consistency tests, in the form of constraints on the calculated coefficients, follow from the integrals

$$\int_0^\infty \frac{W_k^j}{(j-1)!} x^{j-1} e^{-W_k x} dx = 1, \quad \int_0^\infty \frac{W_k^j}{(j-1)!} x^j e^{-W_k x} dx = \frac{j}{W_k}.$$

The first follows from the fact that the integral of $p_{\boldsymbol{w}}(x)$ is unity

$$\sum_{k=1}^{K} \sum_{j=1}^{q_k} \frac{(-1)^{q_k-j} B_{q_k-j}\left(C_1^k, C_2^k, \ldots, C_{q_k-j}^k\right) A_k}{(q_k-j)!} = 1 \tag{C5}$$

and the second from the fact that the first moment of $p_{\boldsymbol{w}}(x)$ is easily calculated from the definition of S_M,

$$\sum_{k=1}^{K} \sum_{j=1}^{q_k} \frac{(-1)^{q_k-j} B_{q_k-j}\left(C_1^k, C_2^k, \ldots, C_{q_k-j}^k\right) A_k}{(q_k-j)!} \frac{j}{W_k} = \sum_{i=1}^{M} \frac{1}{w_m}. \tag{C6}$$

The consistency tests (C5) and (C6) can be used to verify that all coefficients are correct and evaluated to the required precision (see below).

2. The case $M \to \infty$

For the purposes of this work, the PDF $p_{\boldsymbol{w}}^*(x)$ of the modified sum

$$S_M^* = \sum_{m=1}^{M} \frac{X_m - 1}{w_m} \tag{C7}$$

must be evaluated in the limit $M \to \infty$. Notice that the modification ensures that S_M^* has zero mean. In general, the random variable S_∞^* will be well defined provided the sum $\sum_{m=1}^{\infty} w_m^{-2}$ is convergent.

Evidently, the formula (C4) must be approximated at finite M in order to estimate $p_{\boldsymbol{w}}^*(x)$. However, if a crude truncation is used, convergence with increasing M is slow. Slow convergence is particularly problematic because when M is large it is necessary to use high precision arithmetic to evaluate (C4). The high precision requirement is easily confirmed numerically using the consistency tests (C5) and (C6), because a fixed precision calculation will eventually fail the tests as M is increased.

An equally practical, but more rapidly convergent, means of truncating (C4) is by approximating the tail of the sum by a Gaussian random variable with identical mean and variance. In other words, we substitute $S_{\infty,M}^*$ for S_∞^*, where

$$S_{\infty,M}^* = \sum_{m=1}^{M} \frac{X_m - 1}{w_m} + R_M, \tag{C8}$$

where $R_M \sim \mathcal{N}(0, \sigma_M^2)$ is a normally distributed random variable with mean zero and variance $\sigma_M^2 = \sum_{m=M+1}^{\infty} w_m^{-2}$. (In our problem, this approximation can be justified using the CLT, as the number of wave numbers in each shell grows with the truncation wave number.)

The PDF of (C8) is given by a convolution of (C4) (with mean shifted to account for the modification in the sum S_M^* compared with S_M) with the normal distribution, i.e.,

$$p_{\boldsymbol{w}}(x) = \sum_{k=1}^{K} \sum_{j=1}^{q_k} \frac{(-1)^{q_k-j} B_{q_k-j}\left(C_1^k, C_2^k, \ldots, C_{q_k-j}^k\right) A_k}{(q_k - j)!} F_j\left(x + \mu_M, W_k, \sigma_M^2\right), \tag{C9}$$

where $\mu_M = \sum_{m=1}^{M} w_m^{-1}$ and $F_j(x,\lambda,\sigma^2)$ is the convolution of an Erlang random variable with PDF $g_j(x,\lambda)$ [see Eq. (32)] and a normal random variable with zero mean and variance σ^2. An explicit formula for the PDF F_j can be found by direct integration

$$F_j(x,\lambda,\sigma^2) = \frac{\lambda^j \sigma^{j-1} e^{-x^2/2\sigma^2}}{2(j-1)!} \left[\sqrt{\frac{2}{\pi}} \sum_{k=0}^{j-2} (-1)^{j-1-k} \binom{j-1}{k} \mathrm{He}_k^c\left(\frac{x-\lambda\sigma^2}{\sigma}\right) \mathrm{He}_{j-2-k}\left(\frac{x-\lambda\sigma^2}{\sigma}\right) \right.$$
$$\left. + \mathrm{He}_{j-1}^c\left(\frac{x-\lambda\sigma^2}{\sigma}\right) e^{(x-\lambda\sigma^2)^2/2\sigma^2} \mathrm{erfc}\left(-\frac{x-\lambda\sigma^2}{\sqrt{2}\sigma}\right) \right], \tag{C10}$$

where $\mathrm{He}_k(\cdot)$ denotes the kth (probabilistic) Hermite polynomial, $\mathrm{He}_k^c(x) = \mathrm{He}_k(ix)/i^k$, and $\mathrm{erfc}(\cdot)$ is the complementary error function.

APPENDIX D: ASYMPTOTICS AS $\varepsilon \to \infty$

The statistics in the limit $\varepsilon \to \infty$ can be obtained by differentiating (38) to obtain

$$\partial_\varepsilon \langle E_{\boldsymbol{k}} \rangle = [\beta_k - \beta(\varepsilon)] \langle E_{\boldsymbol{k}} \rangle + 1, \tag{D1}$$

where $\beta_k = -4\pi^2 k^2$ are the domain inverse temperatures of $\mathcal{D}$ in the sense of EA [2]. An asymptotic solution to Eq. (D1) can be sought under the constraint of the energy equation in the form

$$\varepsilon = {\sum}' \langle E_{\boldsymbol{k}} \rangle - \beta_k^{-1}, \tag{D2}$$

where the prime denotes the summation over wave numbers defined in Sec. II A. A series solution can be sought in the form (cf. [2])

$$\beta(\varepsilon) = \beta_1 + \sum_{j=1}^{\infty} B_j\, \varepsilon^{-j}, \quad \langle E_{(1,0)} \rangle, \langle E_{(0,1)} \rangle = \frac{\varepsilon}{2} + \sum_{j=0}^{\infty} A_j \varepsilon^{-j}, \quad \langle E_{\boldsymbol{k}} \rangle = \sum_{j=0}^{\infty} A_{\boldsymbol{k},j}\, \varepsilon^{-j} \quad (|\boldsymbol{k}| > 1). \tag{D3}$$

Notice that wave numbers $\boldsymbol{k} = (0,1)^T$ and $\boldsymbol{k} = (1,0)^T$ require a separate treatment as they are the condensate wave numbers in which most of the energy resides in the $\varepsilon \to \infty$ limit.

Inserting the ansatz (D3) into (D1) and (D2) and equating powers of ε^{-1} leads to

$$\beta(\varepsilon) = \beta_1 + \frac{1}{\varepsilon} + O(\varepsilon^{-2}),$$
$$\langle E_{(1,0)} \rangle, \langle E_{(0,1)} \rangle = \frac{\varepsilon}{2} + \sum_{k \neq 1} \frac{q_k \beta_1}{\beta_k(\beta_k - \beta_1)} + O(\varepsilon^{-1}),$$
$$\langle E_{\boldsymbol{k}} \rangle = \frac{1}{\beta_1 - \beta_k} + O(\varepsilon^{-1}) \quad (|\boldsymbol{k}| > 1). \tag{D4}$$

The sum in (D4) is over all unique wave numbers in the doubly periodic lattice except unity, i.e., $k = \{\sqrt{2}, 2, \sqrt{5}, \ldots\}$, and the $\{q_k\}$ are the associated number of wave-number vectors. One interesting result in (D4) is that the caloric curve $\beta(\varepsilon)$ approaches its limiting value $\beta(\varepsilon) \to \beta_1$ from above, rather than from below as was shown to be the case for a bounded domain with a nondegenerate leading eigenvalue. Therefore, the doubly periodic domain apparently does not exhibit negative

specific heat capacity. Further terms in the series solutions can be calculated straightforwardly, following the method of EA [2].

---

[1] D. G. Dritschel, M. Lucia, and A. C. Poje, Equilibrium statistics and dynamics of point vortex flows on the sphere, Phys. Rev. E **91**, 063014 (2015).

[2] J. G. Esler and T. L. Ashbee, Universal statistics of point vortex turbulence, J. Fluid Mech. **779**, 275 (2015).

[3] J. C. McWilliams, The emergence of isolated coherent vortices in turbulent flow, J. Fluid Mech. **146**, 21 (1984).

[4] Z. Xiao, M. Wan, S. Chen, and G. L. Eyink, Physical mechanism of the inverse energy cascade of two-dimensional turbulence: A numerical investigation, J. Fluid Mech. **619**, 1 (2009).

[5] C. Sire and P.-H. Chavanis, Numerical renormalization group of vortex aggregation in 2D decaying turbulence: The role of three-body interactions, Phys. Rev. E **61**, 6644 (2000).

[6] C. Sire, P.-H. Chavanis, and J. Sopik, Effective merging dynamics of two and three fluid vortices: Application to two-dimensional decaying turbulence, Phys. Rev. E **84**, 056317 (2011).

[7] R. Benzi, M. Colella, M. Briscolini, and P. Santangelo, A simple point vortex model for two-dimensional decaying turbulence, Phys. Fluids **4**, 1036 (1992).

[8] D. G. Dritschel, R. K. Scott, C. Macaskill, G. A. Gottwald, and C. V. Tran, Unifying Scaling Theory for Vortex Dynamics in Two-Dimensional Turbulence, Phys. Rev. Lett. **101**, 094501 (2008).

[9] T. P. Billam, M. T. Reeves, B. P. Anderson, and A. S. Bradley, Onsager-Kraichnan Condensation in Decaying Two-Dimensional Quantum Turbulence, Phys. Rev. Lett. **112**, 145301 (2014).

[10] T. Simula, M. J. Davis, and K. Helmerson, Emergence of Order from Turbulence in an Isolated Planar Superfluid, Phys. Rev. Lett. **113**, 165302 (2014).

[11] H. Salman and D. Maestrini, Long-range ordering of topological excitations in a two-dimensional superfluid far from equilibrium, Phys. Rev. A **94** 043642 (2016).

[12] R. K. Scott (private communication).

[13] L. Onsager, Statistical hydrodynamics, Nuovo Cimento **6**, 279 (1949).

[14] G. Joyce and D. Montgomery, Negative temperature states for a two-dimensional guiding center plasma, J. Plasma Phys. **10**, 107 (1973).

[15] D. Montgomery, W. H. Matthaeus, W. T. Stribling, D. Martinez, and S. Oughton, Relaxation in two dimensions and the "sinh-Poisson" equation, Phys. Fluids **4**, 3 (1992).

[16] Y. B. Pointin and T. S. Lundgren, Statistical mechanics of two-dimensional vortices in a bounded container, Phys. Fluids **19**, 1459 (1976).

[17] J. B. Weiss and J. C. McWilliams, Nonergodicity of point vortices, Phys. Fluids A **3**, 835 (1991).

[18] A. I. Khinchin, *Mathematical Foundations of Statistical Mechanics* (Dover, New York, 1949).

[19] K. Khanin, Quasi-periodic motion of vortex systems, Physica D **4**, 261 (1982).

[20] C. C. Lim, Existence of KAM tori in the phase-space of lattice vortex systems, Z. Angew. Math. Phys. **41**, 227 (1990).

[21] C. C. Lin, On the Motion of Vortices in Two Dimensions: I. Existence of the Kirchhoff-Routh Function, Proc. Natl. Acad. Sci. USA **27**, 570 (1941).

[22] R. H. Kraichnan, Statistical dynamics of two-dimensional flow, J. Fluid Mech. **67**, 155 (1975).

[23] P. J. Prince and J. R. Dorman, High order embedded Runge-Kutta formulae, J. Comput. Appl. Math. **7**, 67 (1981).

[24] T. L. Ashbee, J. G. Esler, and N. R. McDonald, Generalized Hamiltonian point vortex dynamics on arbitrary domains using the method of fundamental solutions, J. Comput. Phys. **246**, 289 (2013).

[25] D. G. Crowdy, On rectangular vortex lattices, Appl. Math. Lett. **23**, 34 (2010).

[26] L. J. Campbell, M. M. Doria, and J. B. Kadtke, Energy of infinite vortex lattices, Phys. Rev. A **39**, 5436 (1989).

[27] J. G. Esler, T. L. Ashbee, and N. R. Mcdonald, Statistical mechanics of a neutral point-vortex gas at low energy, Phys. Rev. E **88**, 012109 (2013).
[28] H. Jasiulewicz and W. Kordecki, Convolutions of Erlang and of Pascal distributions with applications to reliability, Demonstr. Math. **36**, 231 (2003).
[29] L. J. Campbell and K. O'Neil, Statistics of two-dimensional point vortices and high-energy vortex states, J. Stat. Phys. **65**, 495 (1991).
[30] J. Miller, Statistical Mechanics of the Euler Equation in Two Dimensions, Phys. Rev. Lett. **65**, 2137 (1990).
[31] R. Robert and J. Sommeria, Statistical equilibrium states for two-dimensional flows, J. Fluid Mech. **229**, 291 (1991).
[32] Z. Yin, D. C. Montgomery, and H. J. H. Clercx, Alternative statistical-mechanical descriptions of decaying two-dimensional turbulence in terms of "patches" and "points", Phys. Fluids **15**, 1937 (2003).